STABILITY OF A TROPICAL MODEL INCLUDING
# SHEAR, SURFACE FRICTION AND CISK HEATING

Terry Gene Robertson

NAVAL POSTGRADUATE SCHOOL
Monterey, California
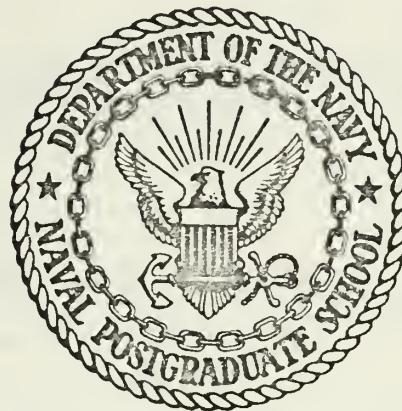
THESIS

STABILITY OF A TROPICAL MODEL INCLUDING SHEAR,
SURFACE FRICTION AND CISK HEATING

by

Terry Gene Robertson

Thesis Advisor: R.T. Williams

March 1973

Stability of a Tropical Model Including Shear,

Surface Friction and CISK Heating

by

Terry G. Robertson
Lieutenant, United States Navy
B.S., Oregon State University,1967

Submitted in partial fulfillment of the
requirements for the degree of

MASTER OF SCIENCE IN METEOROLOGY

from the

NAVAL POSTGRADUATE SCHOOL
March 1973

ABSTRACT

The structure of barotropically unstable disturbances
in the tropics is studied with a two-level quasi-geostrophic
model. An Ekman layer is attached to the lower boundary.
The equations are linearized and the most unstable mode is
found numerically by use of the initial value technique.
CISK heating, horizontal friction and shear are introduced
to give more realistic solutions. Computations are made for
two shear zone wind profiles. The first is represented by
$\bar{U}_1 = \bar{U}_3 = -U_o \tanh y/y_o$ and the second is a mirror reflection
of the first and is given by $\bar{U}_3 = -\bar{U}_1$. The model is run
for 142 days after which growth rates are determined as a
function of the non-dimensional wave number ky_o. The
associated phase angles and amplitudes for the wave numbers
with maximum growth rates are given. The solutions with
heating do not have a strongly preferred mode of maximum
growth.

TABLE OF CONTENTS

TABLE OF SYMBOLS AND ABBREVIATIONS

A_e Vertical Eddy Viscosity

A_H Horizontal Eddy Viscosity

β Derivative of Coriolis parameter at $y = 0$

c_p Specific heat at constant pressure

f_o Coriolis parameter at $y = 0$

g Gravity

ω dp/dt

ψ gz/f_o

R Gas constant for dry air

$\dot{\rho}$ Density

$\overline{T}$ Average temperature from the standard atmosphere

σ $(R^2\overline{T}/p^2 g)$ $(\partial\overline{T}/\partial z + g/c_p)$

ζ $\nabla^2\psi$

z Height

Q Heating added per unit mass

∇^4 Bi-harmonic operator $(\nabla^2)^2$

α Wind inflow angle

ACKNOWLEDGEMENTS

I. INTRODUCTION

Synoptic scale disturbances in the tropical atmosphere have been recognized for a long time (Palmer 1951, Riehl 1954). This paper is concerned with wave disturbances that occur in the lower troposphere and makes no distinction between easterly waves and equatorial waves. Starr and Wallace (1964) showed that in the lower troposphere these disturbances have a "cold core" structure; the rising air is cooler than the air which is subsiding. Warm core structures at higher levels with significant correlations between temperature and vertical velocity have been found by Chang et al. (1970) and Nitta (1970). Vertical velocities associated with these disturbances in general are rising air to the east of the wave axis and subsidence to the west (Yanai and Nitta, 1967).

The energy source for these waves is not known. Baroclinic instability is unlikely because of the smallness of the Coriolis parameter. Charney (1963) performed a scale analysis which indicated that, in the absence of condensation, large-scale motions in the tropics are governed by the barotropic vorticity equation. Charney (1963) suggested that easterly waves arise from barotropic instability. The spectral analysis of Wallace and Chang (1969) indicate a conversion of kinetic energy from the mean flow to the disturbance.

A third possible energy source for these disturbances is latent heat of condensation.

This mechanism is consistent with observations of warm core structures at upper levels (Chang et al. 1970). This heating has been parameterized by Ooyama (1964), Charney and Eliassen (1964), and Kuo (1965) in such a manner that the condensation heating is proportional to the convergence of moisture in the Ekman layer. This leads to a simple instability which is called Conditional Instability of the Second Kind (CISK). Yamasaki (1969) studied the influence of CISK on linearized disturbances in an atmosphere with vertical shear. The solutions displayed many features that are observed in actual tropical wave disturbances. Holton (1971) has obtained similar results with a model that contains a moving heat source and vertical wind shear. These studies strongly suggest that the tropical disturbances are driven by condensation heating. It is known that the CISK mechanism must have a pre-existing disturbance to organize the convective elements before CISK can operate. This pre-existing disturbance could arise from barotropic instability as was demonstrated by Bates (1970). Kuo (1949) examined the stability characteristics of a barotropic zonal current and found that instability is possible only when the absolute vorticity gradient reverses sign in the region.

The purpose of this thesis is to extend the work done by Williams et. al. (1971) to include cases with CISK heating, horizontal friction and vertical shear. Since the Williams

7

et al. (1971) paper is referenced many times, it will
hereafter be referred to as WSN.

II. THE FORECAST EQUATIONS

The quasi-geostrophic prediction equations will be used as the forecast equations following WSN. It is recognized that the quasi-geostrophic approximation is not very accurate near the Equator, but Matsuno (1966) has shown with a barotropic model that quasi-geostrophic motions are identifiable near the Equator if the wavelength is not too long. Yamasaki (1969) has found that the error is small at 20 degrees latitude in a study with a baroclinic model.

The quasi-geostrophic equations are simplified through the introduction of a two-level model which was also used by Bates (1970). The equations are linearized and solved numerically by the initial value technique. The growth rates and wave structures are then computed.

A simple two-level model is constructed by dividing the atmosphere into four layers with a constant pressure differential of $\Delta p/2$ (Fig. 1), numbered 0 to 4 from top to bottom. The boundary condition at $p = p_t$ is $\omega_0 = 0$, which prohibits vertical propagation of energy. Charney (1969) has shown that such energy propagation is unlikely. At $p = p_0$ the boundary condition is $\omega = \omega_e$ where ω_e is the frictionally induced ω at the top of the Ekman layer. Charney and Eliassen (1949) derived the following expression for ω_e

$$\omega_e = -\rho_4 g \ (\frac{A_e}{2f_o})^{\frac{1}{2}} \sin 2\alpha \zeta_4 \ , \qquad (2.1)$$

where A_e is the kinematic eddy viscosity, α is the surface inflow angle, and ζ_4 is the surface geostrophic vorticity.

Fig. 1 Two-level prediction model

It has been shown by Holton et al. (1971) and Chang (1973) that this expression is reasonably valid as far equatorward as 10 degrees, but may be invalid when close to the Equator or south of the ITCZ. The surface geostrophic vorticity can be approximated by

$$\zeta_4 \simeq \zeta_3 = \nabla^2 \psi_3 \;. \qquad (2.2)$$

The quasi-geostrophic vorticity equation in pressure coordinates with horizontal eddy diffusion is

$$\frac{\partial}{\partial t} \nabla^2 \psi + \mathbb{k} \times \nabla \psi \cdot \nabla (\nabla^2 \psi) + \beta_0 \frac{\partial \psi}{\partial x} - f_0 \frac{\partial \omega}{\partial p} = A_H \nabla^4 \psi \;. \qquad (2.3)$$

Observe that when $\omega = 0$ and $A_H = 0$, (2.3) becomes the barotropic vorticity equation which is sufficient to describe the main instability.

Apply this equation at levels 1 and 3 which gives

$$\frac{\partial}{\partial t} \nabla^2 \psi_1 + \Bbbk x \nabla \psi_1 \cdot \nabla (\nabla^2 \psi_1) + \beta_o \frac{\partial \psi_1}{\partial x} - f_o \frac{\omega_2}{\Delta p} = A_H \nabla^4 \psi_1 \quad , \quad (2.4)$$

$$\frac{\partial}{\partial t} \nabla^2 \psi_3 + \Bbbk x \nabla \psi_3 \cdot \nabla (\nabla^2 \psi_3) + \beta_0 \frac{\partial \psi_3}{\partial x} - f_o \frac{(\omega_4 - \omega_2)}{\Delta p} = A_H \nabla^4 \psi_3 \quad .$$

$$(2.5)$$

If it is desired to stop at some intermediate point, say the tropopause, rather than to include the entire atmosphere, smaller layers could be used.

Next consider the quasi-geostrophic first law of thermodynamics in the form

$$\frac{\partial}{\partial t} \frac{\partial \psi}{\partial p} + \Bbbk x \nabla \psi \cdot (\frac{\partial \psi}{\partial p}) + \frac{\sigma}{f_o} \omega = \frac{-\mu^2 K Q_2}{2 f_o} \quad , \quad (2.6)$$

where

$$\sigma = \frac{R^2 \overline{T}}{p^2 g} \left[\frac{\partial \overline{T}}{\partial z} + \frac{g}{C_p} \right] \quad , \quad (2.6a)$$

and $\overline{T}$ is the temperature obtained from the standard atmosphere.

The heating follows the formulation of Ooyama (1964), Charney and Eliassen (1964), and Kuo (1965), i.e., the condensation heating is proportional to the convergence of moisture in the Ekman layer. The form used was given by Ogura (1964)

$$Q_2 = \frac{1}{2} \frac{C_p T}{\overline{\theta}} \frac{\partial \overline{\theta}}{\partial p} \eta \omega_4 \quad , \tag{2.7}$$

where η is a non-dimensional parameter. This relationship
is used in both rising and subsiding air since a Fourier
expansion in x is used; therefore the amplitude of heating
is divided by two.

When (2.6) is applied at level 2 the result is

$$\frac{\partial}{\partial t} (\psi_1 - \psi_3) + \mathbb{k} \times \nabla(\frac{\psi_1 + \psi_3}{2}) \cdot \nabla(\psi_1 - \psi_3) - \frac{\Delta p \sigma_2 \omega_2}{f_o} = \frac{-\mu^2 K Q_2}{2 f_o} \quad . \tag{2.8}$$

Define the following quantities

$$\psi_M = \frac{\psi_1 + \psi_3}{2} \quad , \tag{2.9}$$

$$\psi_T = \frac{\psi_1 - \psi_3}{2} \quad , \tag{2.10}$$

which implies that

$$\psi_1 = \psi_M + \psi_T \quad , \tag{2.11}$$

$$\psi_3 = \psi_M - \psi_T \quad . \tag{2.12}$$

Here ψ_T is proportional to the layer thickness and is there-
fore a measure of the mean temperature in the layer. Use
these definitions, add (2.4) and (2.5) and divide the result
by two, which gives

$$\frac{\partial}{\partial t} \nabla^2 \psi_M + \Bbbk x \nabla \psi_M \cdot \nabla(\nabla^2 \psi_M) + \Bbbk x \nabla \psi_T \cdot \nabla(\nabla^2 \psi_T)$$

$$+ \beta_0 \frac{\partial \psi_M}{\partial x} - \frac{f_0 \omega_4}{2 \Delta p} = A_H \nabla^4 \psi_M \quad . \tag{2.13}$$

For the second forecast equation, subtract (2.5) from (2.4) and eliminate ω_2 with the use of (2.8) which gives

$$\frac{\partial}{\partial t} (\nabla^2 - \mu^2) \psi_T + \Bbbk x \nabla \psi_M \cdot \nabla(\nabla^2 - \mu^2) \psi_T + \Bbbk x \nabla \psi_T \cdot \nabla(\nabla^2 \psi_M)$$

$$+ \beta_0 \frac{\partial \psi_T}{\partial x} + \frac{f_0 \omega_4}{2 \Delta p} = \frac{-\mu^2 K Q_2}{2 f_0} + A_H \nabla^4 \psi_T \quad , \tag{2.14}$$

where

$$\mu^2 = \frac{2 f_0^2}{p^2 \sigma_2} \tag{2.14a}$$

These are the prediction equations for the model. To linearize the equations, the flow is separated into an east-west current that varies only in y, and a small departure from this flow. Thus it is possible to treat waves in x independently and the fields can be defined as follows

$$\psi_M = E(y) + A(y,t) \cos kx + B(y,t) \sin kx \quad , \tag{2.15}$$

$$\psi_T = F(y) + C(y,t) \cos kx + D(y,t) \sin kx \quad , \tag{2.16}$$

13

where k is the x wave number. The coefficients A through D are Fourier amplitudes of the disturbance and E and F are the coefficients of the mean zonal fields.

Substitute the expressions for ψ_M and ψ_T into (2.13), separate the various sine and cosine terms, and neglect all products of the quantities A through D. Equate the coefficients of the cosine terms which gives

$$\frac{\partial}{\partial t} (\frac{\partial^2 A}{\partial y^2} - Ak^2) = k [\frac{\partial E}{\partial y} \frac{\partial^2 B}{\partial y^2} + \frac{\partial F}{\partial y} \frac{\partial^2 D}{\partial y^2} - \frac{\partial^3 E}{\partial y^3} B - \frac{\partial^3 F}{\partial y^3} D$$

$$- k^2(\frac{\partial E}{\partial y} B + \frac{\partial F}{\partial y} D)] - \beta_o Bk - K(\frac{\partial^2}{\partial y^2} - k^2)(A - C)$$

$$+ A_H(\frac{\partial^4 A}{\partial y^4} - 2k^2 \frac{\partial^2 A}{\partial y^2} + k^4 A) \quad , \tag{2.17}$$

The sine terms give

$$\frac{\partial}{\partial t} (\frac{\partial^2 B}{\partial y^2} - Bk^2) = k [- \frac{\partial E}{\partial y} \frac{\partial^2 A}{\partial y^2} - \frac{\partial F}{\partial y} \frac{\partial^2 C}{\partial y^2} + \frac{\partial^3 E}{\partial y^3} A + \frac{\partial^3 F}{\partial y^3} C$$

$$+ k^2(\frac{\partial E}{\partial y} A + \frac{\partial F}{\partial y} C)] + \beta_o Ak - K(\frac{\partial^2}{\partial y^2} - k^2)(B - D)$$

$$+ A_H(\frac{\partial^4 B}{\partial y^4} - 2k^2 \frac{\partial^2 B}{\partial y^2} + k^4 B) \quad . \tag{2.18}$$

14

Repeat the procedure for (2.14) for the cosine terms which gives

$$\frac{\partial}{\partial t} (\frac{\partial^2 C}{\partial y^2} - Ck^2 - C\mu^2) = k [\frac{\partial E}{\partial y} \frac{\partial^2 D}{\partial y^2} + \frac{\partial F}{\partial y} \frac{\partial^2 B}{\partial y^2} - \frac{\partial E}{\partial y} D(k^2 + \mu^2)$$

$$- \frac{\partial F}{\partial y} B(k^2 - \mu^2) - \frac{\partial^3 E}{\partial y^3} D - \frac{\partial^3 F}{\partial y^3} B] - \beta_0 Dk$$

$$+ (K - S)(\frac{\partial^2}{\partial y^2} - k^2)(A - C) + A_H(\frac{\partial^4 C}{\partial y^4} - 2k^2 \frac{\partial^2 C}{\partial y^2} + k^4 C) \quad ,$$

$$(2.19)$$

The results for the sine terms are

$$\frac{\partial}{\partial t} (\frac{\partial^2 D}{\partial y^2} - Dk^2 - D\mu^2) = k [\frac{\partial E}{\partial y} C(k^2 + \mu^2) + \frac{\partial F}{\partial y} A(k^2 - \mu^2)$$

$$- \frac{\partial E}{\partial y} \frac{\partial^2 C}{\partial y^2} - \frac{\partial F}{\partial y} \frac{\partial^2 A}{\partial y^2} + \frac{\partial^3 F}{\partial y^3} A + \frac{\partial^3 E}{\partial y^3} C] + \beta_0 Ck$$

$$+ (K - S)(\frac{\partial^2}{\partial y^2} - k^2)(B - D) + A_H(\frac{\partial^4 D}{\partial y^4} - 2k^2 \frac{\partial^2 D}{\partial y^2} + k^4 D) \quad ,$$

$$(2.20)$$

where

$$K = \frac{f_0 g}{2R\theta} (\frac{A_M}{f_0})^{\frac{1}{2}} \quad , \qquad (2.21)$$

and

$$S = \frac{g}{8} \frac{\eta}{|\theta|} \frac{\partial \overline{\theta}}{\partial p} p_o \left(\frac{A_M}{f_o}\right)^{\frac{1}{2}} \frac{1}{f_o} \quad . \tag{2.22}$$

These are the same equations used by WSN except that in their equations $F = 0$, $\eta = 0$, and $A_H = 0$.

It is necessary to derive the computational equation for vertical motion beginning with

$$\omega_2 = \frac{2}{\Delta p \sigma} \left[\frac{\partial \psi_T}{\partial t} + u_m \frac{\partial \psi_T}{\partial x} + v_m \frac{\partial \psi_T}{\partial y} + \frac{KQ_2}{2f_o} \right] , \tag{2.23}$$

where

$$u_m = - \frac{1}{f_o} \frac{\partial \psi_M}{\partial y} \quad , \tag{2.24}$$

$$v_m = \frac{1}{f_o} \frac{\partial \psi_M}{\partial x} \quad . \tag{2.25}$$

Substitute equations (2.24), (2.25) and (2.16) into (2.23), collect terms, and again neglect all products of A through D which gives

$$\omega_2 = \frac{2}{\Delta p \sigma} \left\{ \cos kx \left[\frac{\partial C}{\partial t} - \frac{k}{f_o} \left(\frac{\partial E}{\partial y} D - \frac{\partial F}{\partial y} B \right) \right] \right.$$

$$\left. + \sin kx \left[\frac{\partial D}{\partial t} + \frac{k}{f_o} \left(\frac{\partial E}{\partial y} C - \frac{\partial F}{\partial y} A \right) \right] + \frac{\partial F}{\partial t} + \frac{KQ_2}{2f_o} \right\} \quad .$$

$$\tag{2.26}$$

16

Both the disturbance and the average vertical motion are given by this equation. The prediction equations and the vertical motion equations are now in the form to be used in the model.

III.   BOUNDARY CONDITIONS AND FINITE
DIFFERENCING SCHEME

The finite difference scheme that was used is illustrated below with a sample variable M_i:

$$\frac{\partial M}{\partial y} = \frac{1}{2H} (M_{i+1} - M_{i-1}), \tag{3.1}$$

$$\frac{\partial^2 M}{\partial y^2} = \frac{1}{H^2} (M_{i+1} - 2M_i + M_{i-1}), \tag{3.2}$$

$$\frac{\partial^3 M}{\partial y^3} = \frac{1}{2H^3}[(M_{i+2} - 2M_{i+1} - M_i) - (M_i - 2M_{i-1} + M_{i-2})]. \tag{3.3}$$

where i is the grid index and H is the distance between grid points.

Centered time differences were used for all quantities except those involving friction and heating. The friction and heating terms were computed at time $(t - \Delta t)$. Initially a forward time step was used. The second order equations for time tendencies were solved by the exact method of Richtmyer (1957, p. 101).

Yanai and Nitta (1968a) studied the problem of using finite difference approximations to solve dynamic instability problems of non-divergent barotropic currents. They showed that for either symmetric or anti-symmetric zonal currents, the exact boundary conditions can be replaced by

placing rigid boundary conditions at a distance equal to
one-half the width of the shearing wind belt. Therefore
rigid boundaries are placed at $y = -W/2$ and $y = W/2$, where
W is the total width of the computational field. Except
for the E and F fields, all variables have the boundary
condition $A = B = C = D = 0$ at $y = \pm W/2$. Second derivatives
that are required on the boundary are set equal to zero.

Fig. 2 Mean wind profile $\overline{U} = -U_o \tanh y/y_o$

20

IV. WIND PROFILE AND INITIAL CONDITIONS

WSN investigated the structure of tropical disturbances
using a similar model and the wind profile ($U = -U_o \tanh y/y_o$).
It is proposed to expand on that paper to include a sinusoidal
profile for an initial disturbance and a thermal wind field
which will be a mirror image of the mean wind field used
by WSN.

If the waves are to grow, the zonal wind profile must
be barotropically unstable. Charney (1963) suggested that
a shear zone could be formed by the transport of angular
momentum from different regions. This would occur when the
Intertropical Convergence Zone is shifted away from the
Equator. The unstable profile chosen to represent this is

$$\bar{U}_1 = \bar{U}_3 = -U_o \tanh y/y_o, \qquad (4.1)$$

which is illustrated in Figure 2. To represent a thermal
wind field the unstable profile is

$$\bar{U}_1 = -\bar{U}_3 = U_o \tanh y/y_o. \qquad (4.2)$$

Lipps (1970) has used the profile represented by (4.1)
in an inviscid study of barotropic instability in the tropics.
This wind field is anti-symmetric with respect to the
Intertropical Convergence Zone, located at $y = 0$.

For the experiments which have the wind profile (4.1), a range of non-dimensional wave numbers (ky_o) from 0.10 to 3.00 will be used. This wide range of wave numbers is necessary because it is uncertain which wave number will be the most unstable mode. Those experiments with the (4.2) wind profile will be run over a range of 0.10 to 1.20. One experiment with the latter wind profile containing CISK heating was run over a wave number range of 0.10 to 3.00.

ψ_M is introduced into the model as a sinusoidal disturbance in y and ψ_T grows from zero as a result of the Ekman friction term. CISK heating is added which greatly increases the growth rates of all fields, particularly the short waves. Horizontal friction is also added. This represents a mixing of the smaller scale waves and smooths out perturbations in the vertical velocity field. Thus at time t = 0

$$A = \sin \frac{\pi y}{W} \tag{4.3}$$

$$B = 0 \tag{4.4}$$

$$C = 0 \tag{4.5}$$

$$D = 0 \tag{4.6}$$

$$E = f_o \, U_o \, y_o \, \ln[\cosh (y/y_o)] \quad \text{or} \quad 0 \tag{4.7}$$

$$F = -f_o \, U_o \, y_o \, \ln[\cosh (y/y_o)] \quad \text{or} \quad 0 \tag{4.8}$$

V. COMPUTATIONAL PROCEDURE

The following constants were used in all computations except those related to heating and friction which were zero if the heating and/or the friction are neglected:

p_o =   100 centibars,

y_o =   400 or 200 or 100 kilometers,

W =   4000 kilometers,

U_o =   10 meters per second,

f_o = 5×10^{-5} per second,

σ =   0.4 meters per second squared per centibar squared,

β =   0.0 or 2.29×10^{-11} per meter per second,

Δp =   50 centibars,

A_e =   10 meters per second squared,

A_H = 1×10^5 meters per second squared,

α =   22.5 degrees,

μ^2 = 2.49×10^{-12} per meter squared,

H =   50 or 25 or 12.5 kilometers,

Δt =   1.0 or 0.5 or 0.25 hours,

η =   2.0 or 1.0,

$\partial\bar{\theta}/\partial p$ =   -0.6 degrees per centibar.

A forecast period of 142 days was used so that the most un-stable mode would have reached the maximum growth rate. For most cases, it was found that the growth rate at 110 days was the same as the growth rate at the longer period.

WSN introduced a random disturbance into the ψ_M field. It was found that by using a sinusoidal profile for the disturbance, similar growth rates were obtained except in the cases where heating was added. The sinusoidal profile was used as the disturbance field for all experiments with variations of $\bar{U}$, β, CISK heating, horizontal and surface friction, and the non-dimensional wave number (ky_o). Growth rates were then computed by assuming the amplitude could be written as

$$a_1 = a_o \exp(nU_o/y_o) \, t_1, \tag{5.1}$$

$$a_2 = a_o \exp(nU_o/y_o) \, t_2, \tag{5.2}$$

where n is the growth rate and a_o is a constant. If the ratio a_2/a_1 is formed, the growth rate can be shown to be

$$n = \frac{y_o \, \ln(a_2/a_1)}{U_o(t_2 - t_1)} . \tag{5.3}$$

The dimensional doubling time is

$$T = \frac{y_o \, \ln 2}{nU_o} . \tag{5.4}$$

VI. RESULTS

A series of experiments were conducted over a wide
variety of conditions. The total distance over the grid
was 4000 km. A grid mesh size of 50 km and a time step of
1.0 hours was used for all experiments except two cases.
In one case a grid mesh of 25 km with a 0.5 hour time step
was used and in the other case a grid mesh of 12.5 km and
a 0.25 hour time step was used.

The more important experiments are given in Table 1 as
a function of $\bar{U}$, β, heat, friction, and ky_0. The growth
rate n is also given. The table shows whether or not CISK
heating and horizontal friction were included for each
experiment. All experiments given in Table 1 included
surface friction. For each experiment, calculations were
made to determine the non-dimensional growth rate as a
function of the non-dimensional wave number ky_0 so that the
results could be compared to those obtained by WSN. The
value of ky_0 that was associated with the maximum growth
rate is shown in the table.

It should be mentioned that the value used for the non-
dimensional heating parameter η was too large. A more
realistic value for η would have been 1.0 instead of 2.0.
Test runs were made for experiments 1 through 4 with
$\eta = 1.0$ and in all cases, the growth rates were reduced to
about one-third the value obtained with the larger value
of η.

25

Table 1. Compilation of numerical experiments

Exp	$\bar{U}$	β	n	Heating	Friction	ky_o
1	$\bar{U}_1 = \bar{U}_3$	0	0.770	Yes	No	0.40
2	$\bar{U}_1 = \bar{U}_3$	2.29×10^{-11}	0.730	Yes	No	0.40
3	$\bar{U}_1 = \bar{U}_3$	0	0.520	Yes	Yes	0.40
4	$\bar{U}_1 = \bar{U}_3$	2.29×10^{-11}	0.520	Yes	Yes	0.40
5	$\bar{U}_1 = -\bar{U}_3$	0	0.283	No	No	0.65
6	$\bar{U}_1 = -\bar{U}_3$	0	0.790	Yes	No	1.10

Experiment 1 was run with the (4.1) wind profile and included CISK heating and surface friction. The beta term and horizontal friction were excluded. Garcia (1956) found that the shear zone profile (4.1) is barotropically unstable when $0 < ky_o < 1$. Betchov and Criminale (1967) computed the eigensolutions for this profile throughout this range and found the maximum instability at $ky_o = 0.45$ which agreed with the results of WSN. The wave number of maximum instability (0.40) agrees quite closely with that value but the growth rate (n = 0.770) is much greater than the value obtained by WSN (n = 0.153) even when the smaller value of η was used. Figure 3 contains the growth rate profile for the full range of wave numbers. The maximum growth rate corresponds to a doubling time of 0.42 days and a wavelength of 6280 km. The sharp irregularities between 0.10 and 1.00

arise because the wave number increment in that region is 0.10 as compared to 0.50 between 1.00 and 3.00. In the non-heating cases of WSN, there was no growth for $ky_o > 1$, but in experiment 1 there is large growth which must be due in part to the CISK process. The Figure shows that the growth is nearly independent of the scale. Figure 4 contains the amplitudes of ψ_T and ω_2 for this experiment. ψ_1 and ψ_3 are not shown for clarity purposes as they have the same magnitude as ψ_T. ψ_1 is slightly larger and ψ_3 slightly less than ψ_T but the shape is identical. The units are arbitrary since the basic equations are linear. However, ω_2 is not plotted on the same scale as ψ_T. All quantities show double maxima with peaks at $y = \pm 1.2$. These results are somewhat similar to those obtained by WSN without heating but their results showed the minimum between peaks as only slightly less than the maximum whereas in Figure 4, the minimum is less than one-half of the maximum. Also the ψ_1, ψ_3, and ψ_T fields are very close together but WSN showed ψ_1 to be predominate. The closeness of the ψ fields roughly implies that the vertical mean streamfunction is nearly zero so the fields are basically of a thermal charac-ter. Figure 5 contains the phase angles for ψ_1, ψ_3, ψ_T, and ω_2 for this experiment as functions of y. ψ_1 and ψ_T are very nearly coincident at the outer edges and $\psi_1 = \psi_T$ between $y = \pm 2$ although only ψ_1 is shown in Figure 5. ψ_3 is approximately 180 degrees out-of-phase from ψ_1 and ψ_T which indicates the pressure trough at the surface is replaced
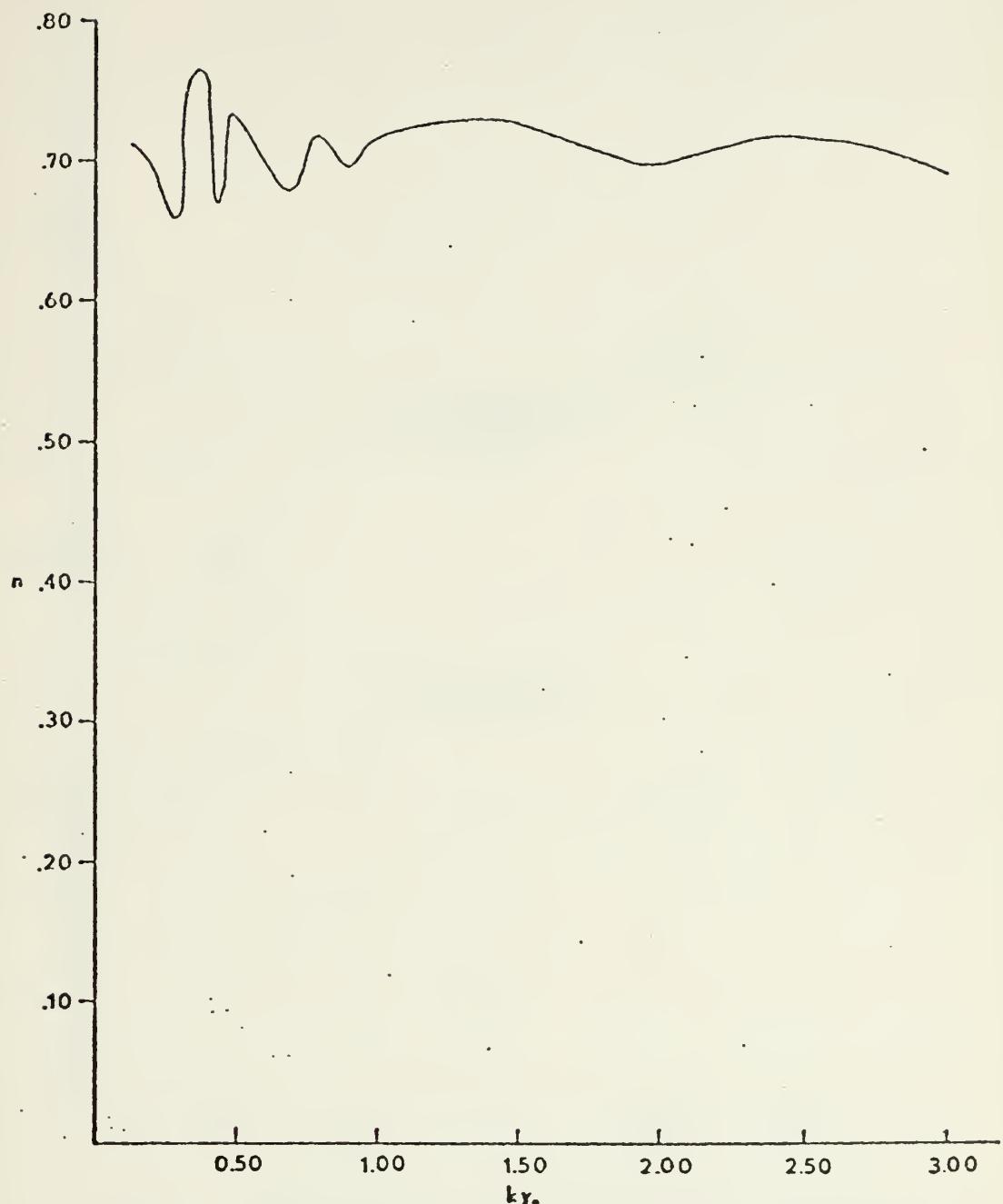
Fig. 3 Growth rates for experiment 1.

28
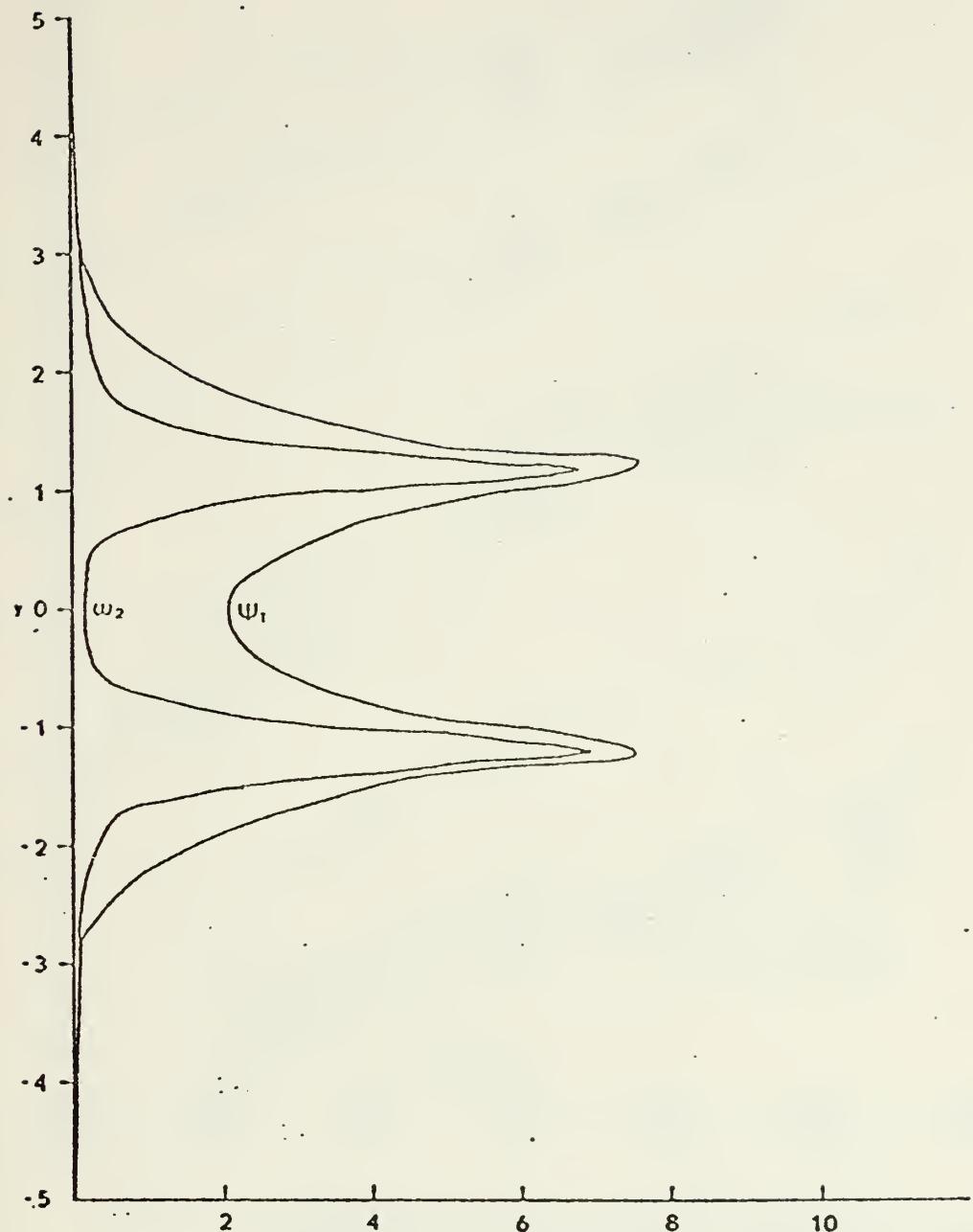
Fig. 4 Amplitudes of ψ_T, and ω_2 for experiment 1. ψ_T and ω_2 are on different scales.
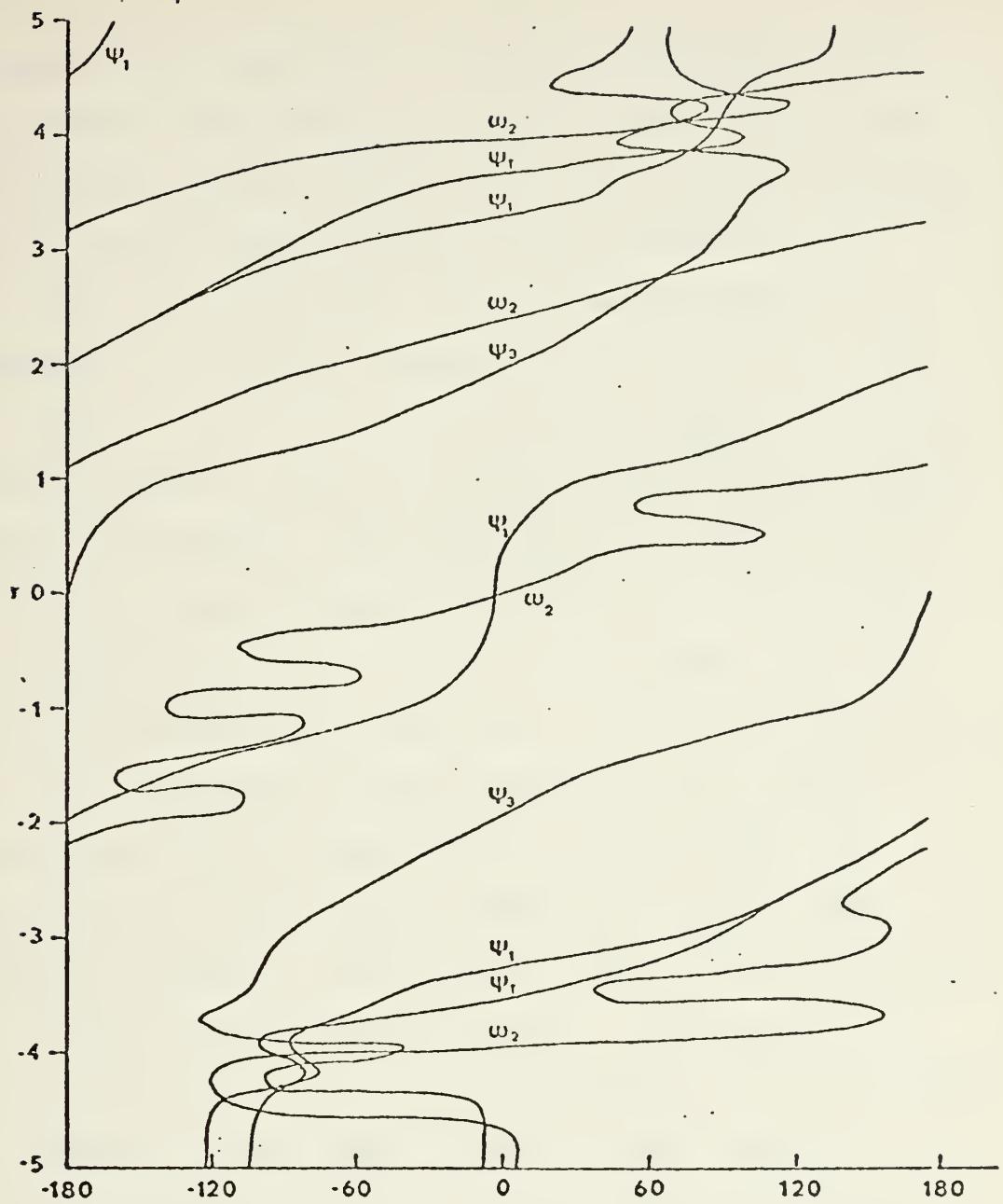
Fig. 5   Phases of ψ_1, ψ_3, ψ_T, and ω_2 for
experiment 1 in degrees. Each dependent
variable is expressed in the form
$P\cos(kx-\delta)$, where P is the amplitude
and δ is the phase angle.

30

by a ridge at the upper level. This is consistent because the Ekman effect and heating are tied to the field at level 3 which produces heating above surface low pressure systems. Unlike the results found by WSN for the adiabatic case, Figure 5 shows the horizontal tilt of the disturbance to be a minimum at $y = 0$ and a maximum at $y = \pm(1$ to $4)$. The general sense of the tilt is northeast but larger than that observed in easterly waves. Also the tilt of the ω_2 field fluctuates considerably. The small perturbations, particularly in the ω_2 field, suggest that there is not a clearly defined unstable mode in y. This does not agree with the results of WSN which had no heating. It is interesting to note that the fields are very smooth but have large gradients except for ω_2 which shows a radical behavior.

Experiment 2 is the same as experiment 1 except the beta term is included. The results in general are the same. Figure 6 shows the growth rate profile. The magnitude of the growth rates is almost the same although a small decrease in the maximum is noted (from 0.770 to 0.730) and the perturbations betwen $ky_o = 0.10$ and 1.00 have been somewhat smoothed. The maximum growth rate corresponds to a doubling time of 0.44 days and a wave length of 6280 km. Figure 7 contains the amplitudes for experiment 2 as a function of y. As in experiment 1, only ψ_T and ω_2 are shown with ψ_T and ω_2 on different scales. Again there is a double maxima at $y = \pm 1.2$ but the profile is asymmetric with the larger maximum in the shear zone to the north. This asymmetry is
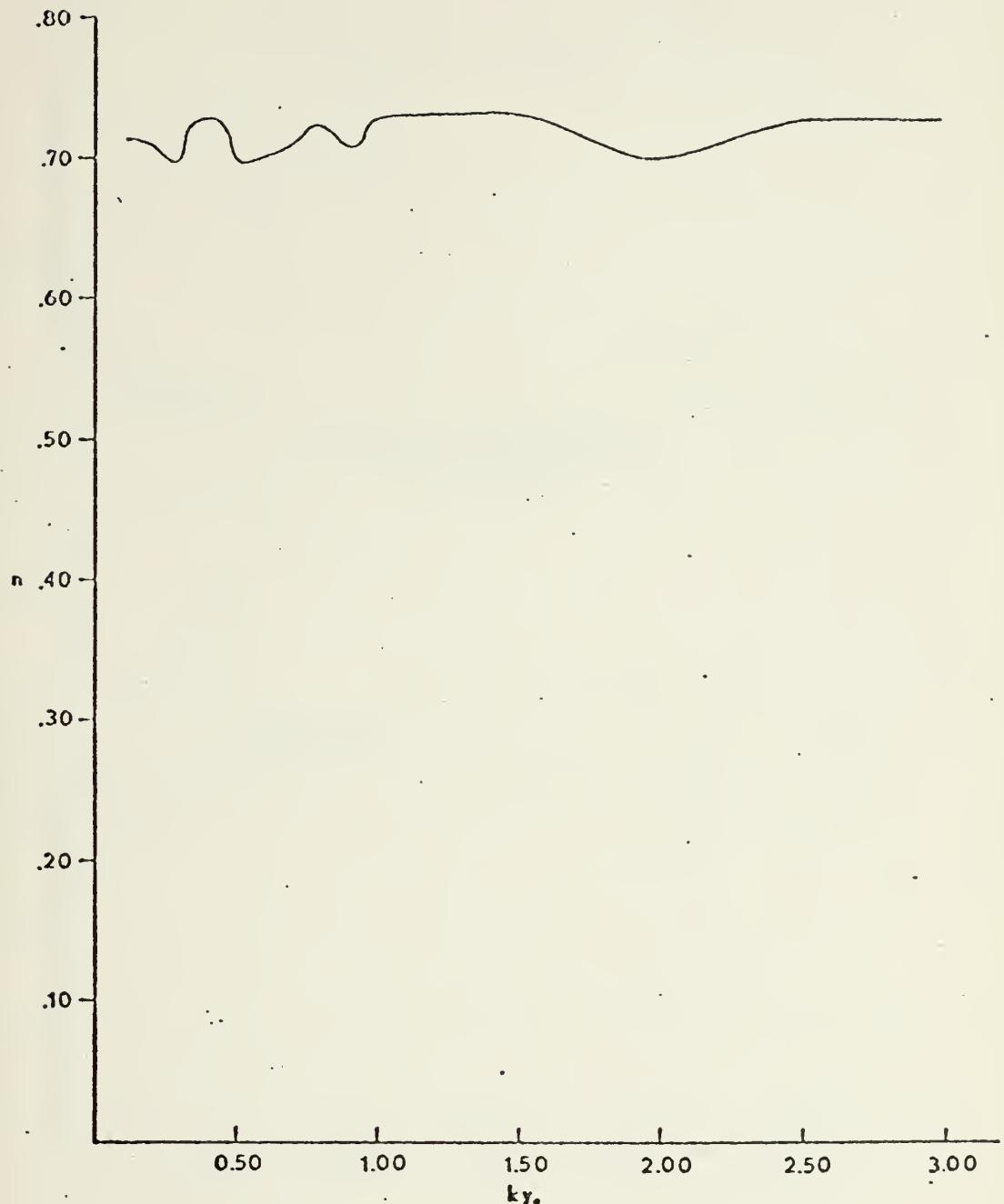
Fig. 6 Growth rates for experiment 2.
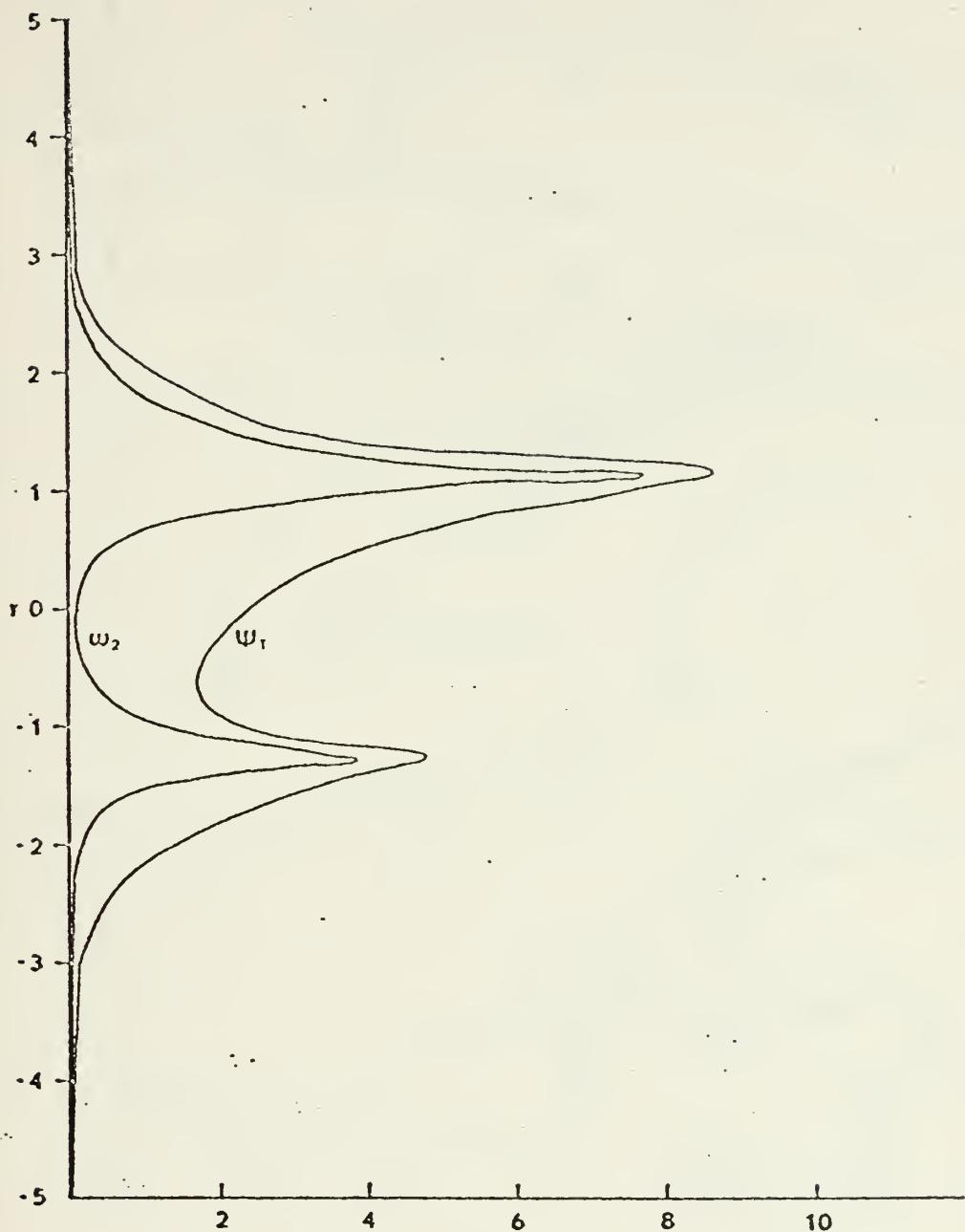
Fig. 7 Amplitudes of ψ_T and ω_2 for experiment 2. ψ_T and ω_2 are on different scales.

33
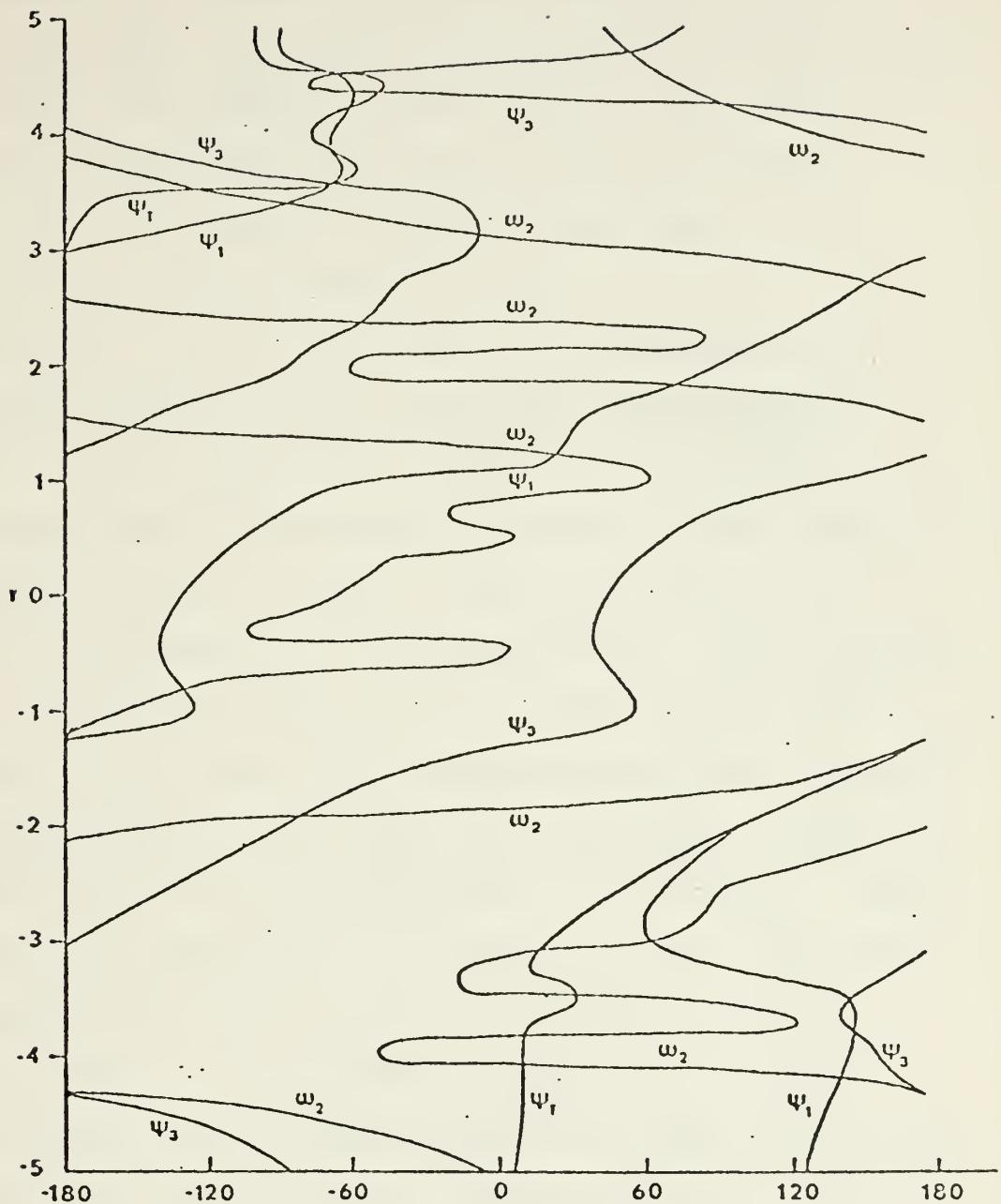
Fig. 8   Phases of ψ_1, ψ_3, ψ_T, and ω_2 for
experiment 2 in degrees. Each dependent
variable is expressed in the form
$P\cos(kx-\delta)$, where P is the amplitude
and δ is the phase angle.

expected since the absolute vorticity gradient is not an odd function of y. WSN found that the shift of symmetry was to the south while Figure 7 shows a shift to the north. The phase relationships of ψ_1, ψ_3, ψ_T, and ω_2 shown in Figure 8 are very similar to those in experiment 1 and again only ψ_1 is shown between y = ±2.

Experiment 3 was run with the (4.1) wind profile and included CISK heating, surface friction, and horizontal friction. The beta term was excluded. The horizontal friction was added in an attempt to smooth out the vertical velocity (ω_2) pattern. Figure 9 shows the growth rate profile for experiment 3. The maximum growth rate has been reduced considerably (from 0.770 to 0.520) and the growth falls off at $ky_o \geq 2.00$. The maximum growth rate corresponds to a doubling time of 0.62 days and a wavelength of 6280 km. Note that there are no perturbations in the profile. Figure 10 contains the amplitudes of ψ_T and ω_2 for this experiment. As in experiment 1, only ψ_T and ω_2 are shown and are on different scales. ψ_1 is slightly larger and ψ_3 slightly smaller than ψ_T. It is interesting to note that the largest amplitudes are located near the boundaries for all fields whereas in the case without friction (experiment 1), the maximum amplitudes are in the central regions. Perhaps the large scale eddies favored by the horizontal friction are heavily damped by the horizontal shear between y = ±1. Figure 11 contains the phases of ψ_1, ψ_3 and ω_2. ψ_T is not shown but it is everywhere equal to ψ_1. Again ψ_T and ψ_3
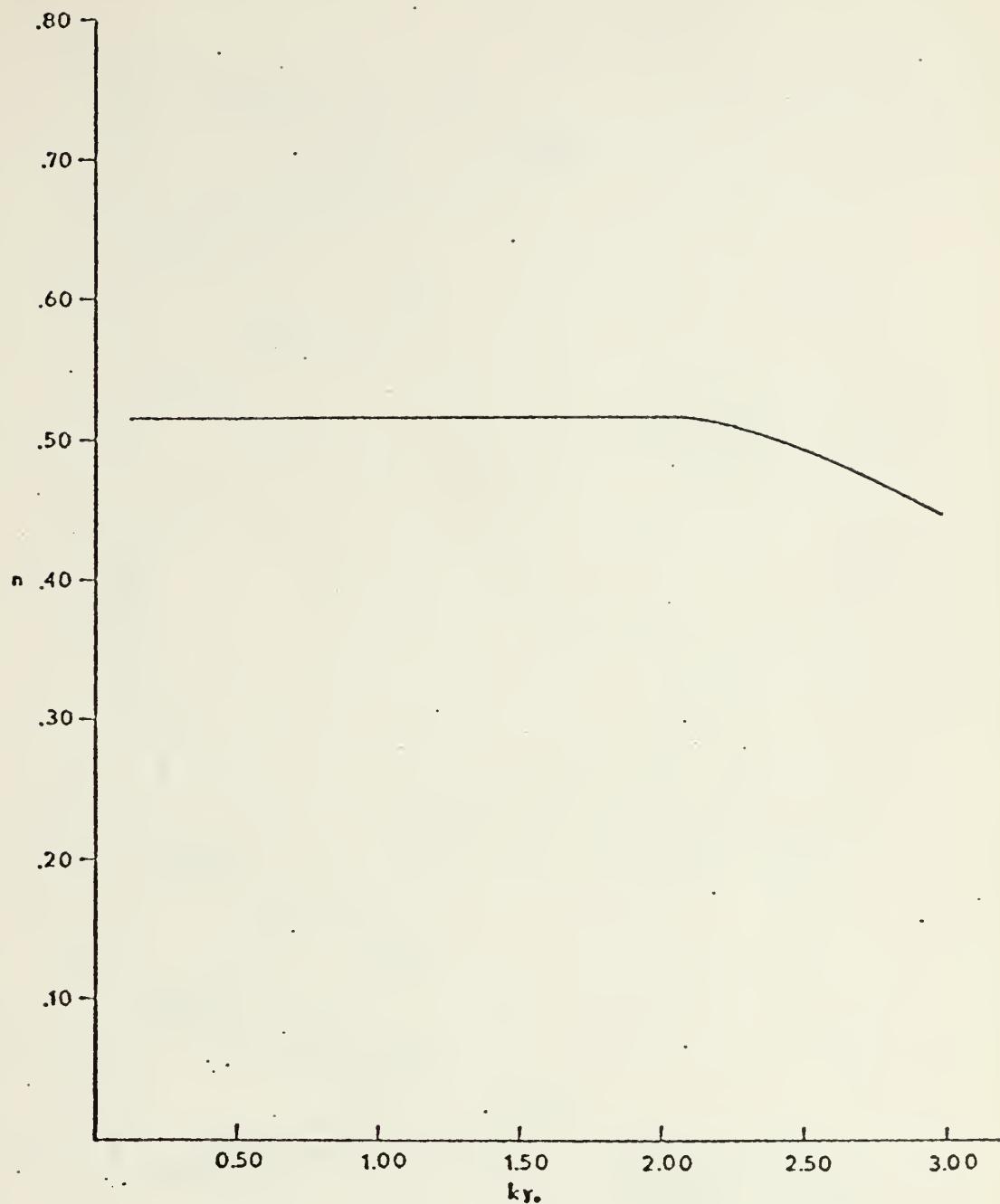
Fig. 9 Growth rates for experiment 3.
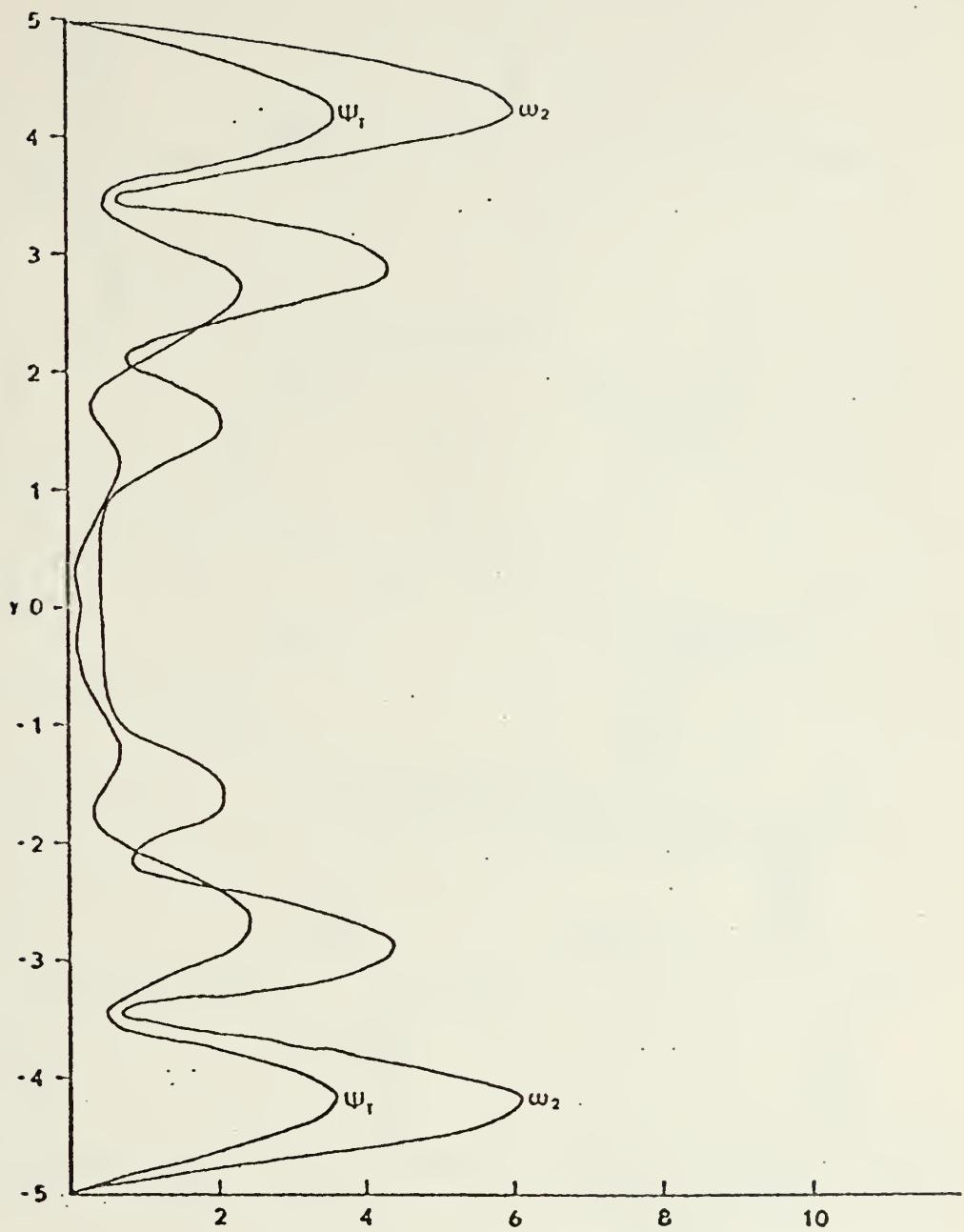
Fig. 10 Amplitudes of ψ_T and ω_2 for experiment 3. ψ_T and ω_2 are on different scales.

37
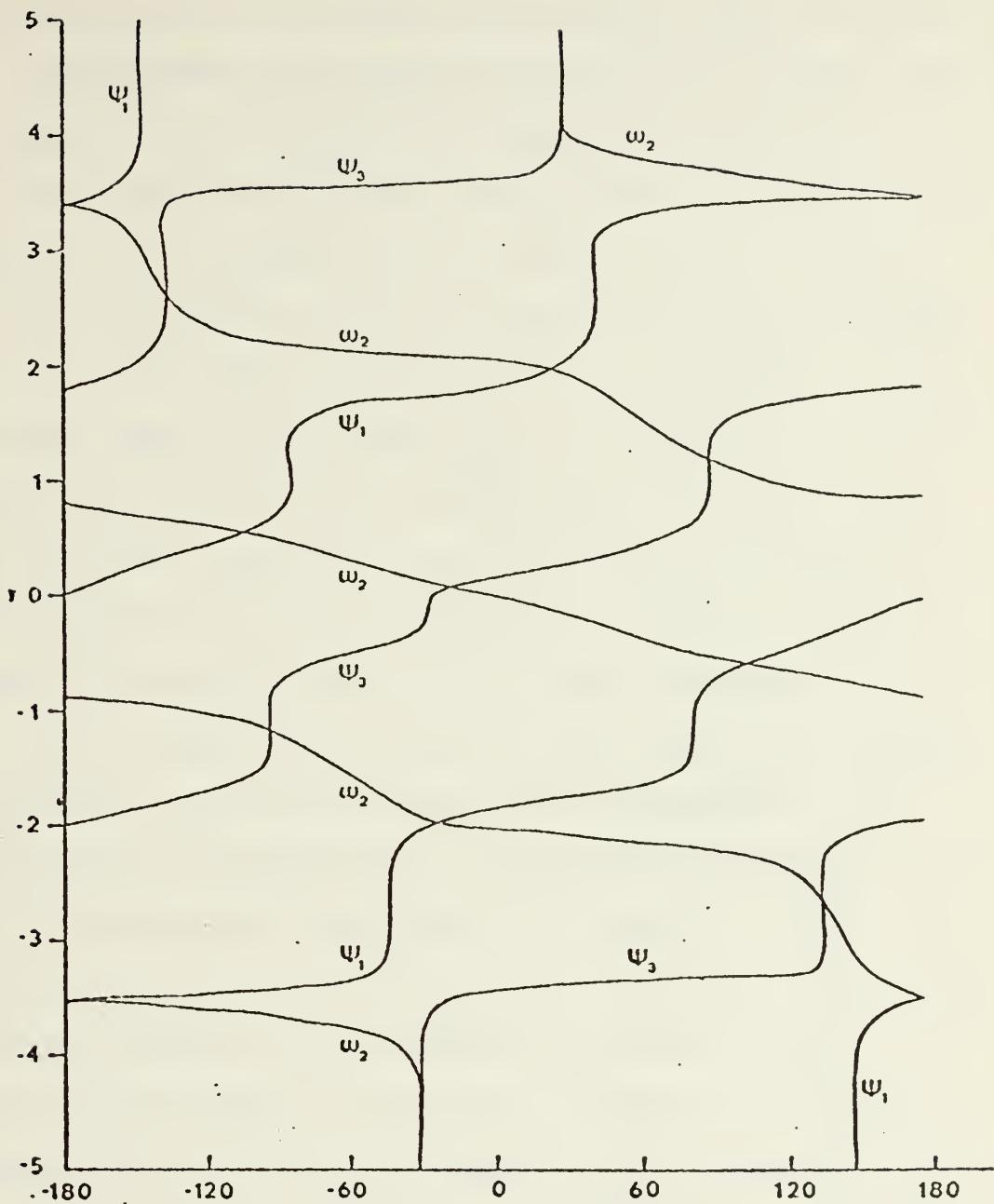
Fig. 11   Phases of ψ_1, ψ_3, and ω_2 for experiment
3 in degrees.   Each dependent variable
is expressed in the form $P\cos(kx-\delta)$,
where P is the amplitude and δ is the
phase angle.

38

are out-of-phase but all fields are smoother than in experiment 1. Where there are peaks in the amplitude fields, the phase angles of ω_2 and ψ_3 are the same which tends to suggest that warm air is rising and cold air is sinking. Again there is an eastward tilt in the ψ fields. The ω_2 field tilt is opposite to the ψ fields but it does correlate with the ψ_3 field where the amplitude is a maximum. It appears the scale in y is about $2y_o$.

Experiment 4 is the same as experiment 3 but the beta term is included. The beta term has very little effect except to make the solutions asymmetric. Figure 12 shows the growth rate profile which is the same as Figure 9 except for the slight perturbation between the wave numbers 0.40 and 0.90. The maximum growth rate corresponds to a doubling time of 0.62 days and a wavelength of 6280 km. Figure 13 contains the amplitudes of ψ_T and ω_2. As in experiment 3, ψ_1 and ψ_3 are not shown. The only change noted is a slight increase in the maximum to the north and a decrease in the maximum to the south. Figure 14 contains the phases of ψ_1, ψ_3 and ω_2 and again ψ_T is everywhere equal to ψ_1. The ω_2 and ψ_3 correlation is the same as in experiment 3.

Experiment 5 was run with (4.2) wind profile and surface friction. Heating and horizontal friction were excluded. This profile is a mirror reflection of the $\overline{U}_1$ profile, that is $-\overline{U}_1$. This profile is similar in general to the wind profile in the Intertropical Convergence Zone where there

is cyclonic shear in the lower region and anticyclonic

shear in the upper region. Since the ITCZ is driven by

heating and convergence, this is the type of mean wind

pattern that is expected. Three cases were run although only

one is shown in the table. Case 1, which is summarized in

Table 1, had a grid mesh of 50 km, a y_o value of 400 km and

a time step of 1.0 hours. Case 2 used a grid mesh of 25 km,

a y_o value of 200 km and a time step of 0.50 hours. Case 3

used a grid mesh of 12.5 km, a y_o value of 100 km and a

time step of 0.25 hours. Case 1 was run over the range of

wave numbers from 0.10 to 1.20 and the maximum unstable

mode was found at ky_o = 0.65. Cases 2 and 3 were run only

at wave number 0.65. Figure 15 shows the growth rate profile

for experiment 5, case 1. The maximum growth rate at ky_o = 0.65

was 0.283. The doubling time was 1.13 days with a wavelength

of 3465 km. For case 2, the growth rate obtained was 0.188

with a doubling time of 0.85 days and a 1930 km wavelength.

For case 3 a growth rate of 0.162 was found with a doubling

time of 0.50 days and a 967 km wavelength. For cases 2 and

3, ky_o = 0.65 may not be the maximum growth rate. This shows

that as the scale (y_o) is decreased, the baroclinic process

is suppressed. This is consistent with baroclinic instab-

bility theory. It is noted that in case 3, the growth rate

is the same as that obtained by WSN in their experiment 1.

Figure 16 contains the amplitudes of ψ_1, ψ_T and ω_2 for case

1. For clarity, ψ_3 is not shown but it is slightly less

than ψ_1. These amplitudes are very similar to those of WSN
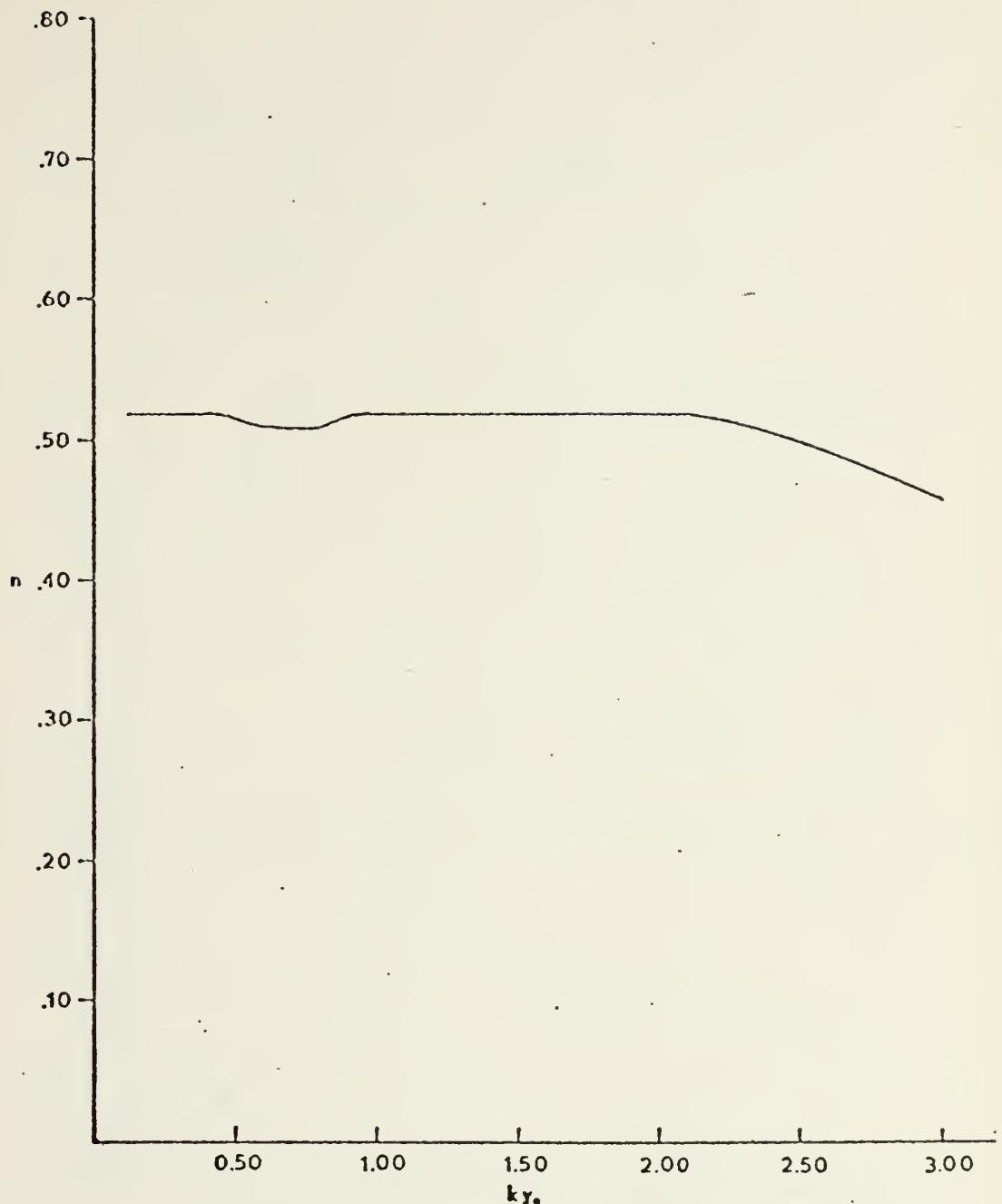
Fig. 12   Growth rates for experiment 4.
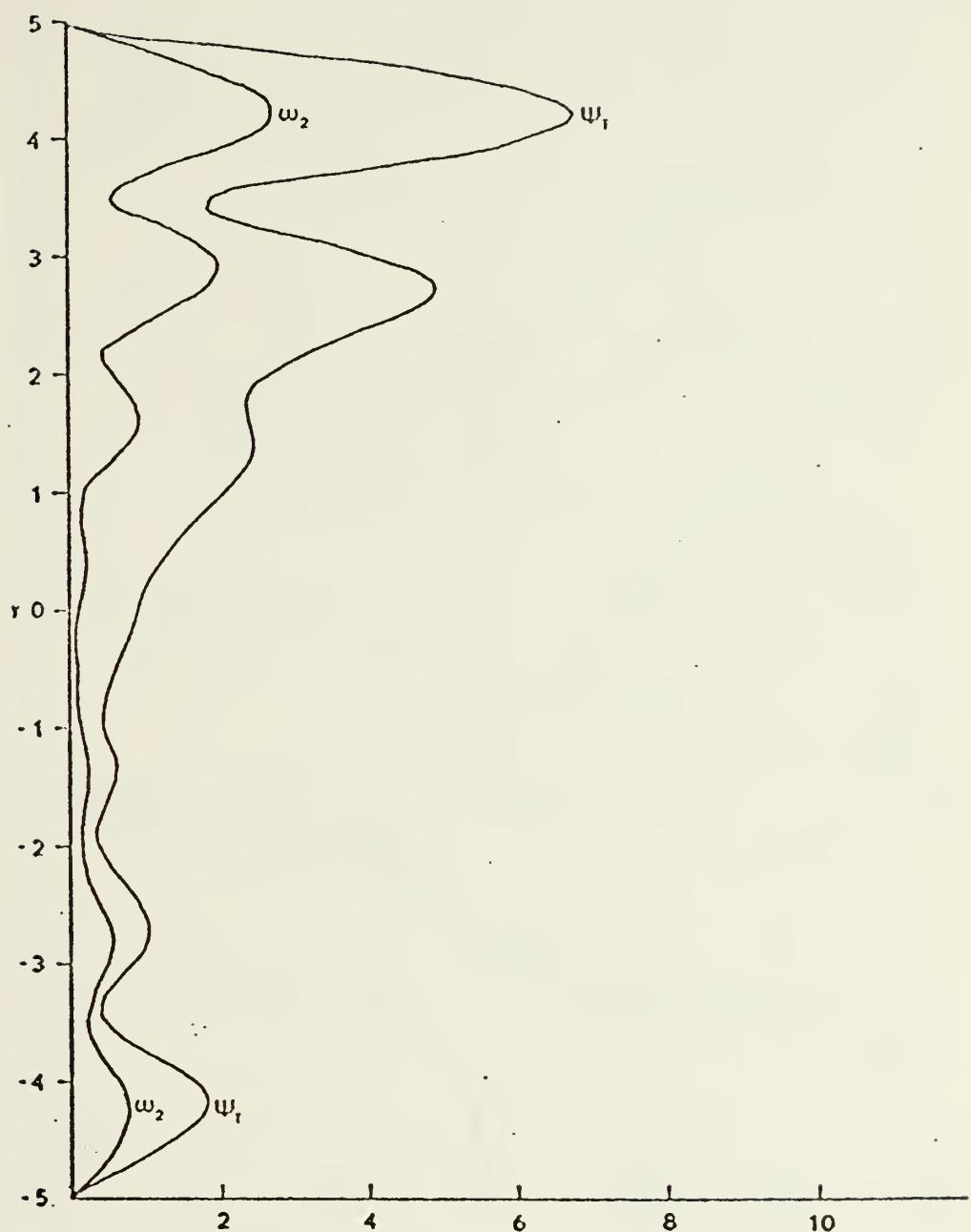
Fig. 13 Amplitudes of ψ_T and ω_2 for experiment
4. ψ_T and ω_2 are on different scales.
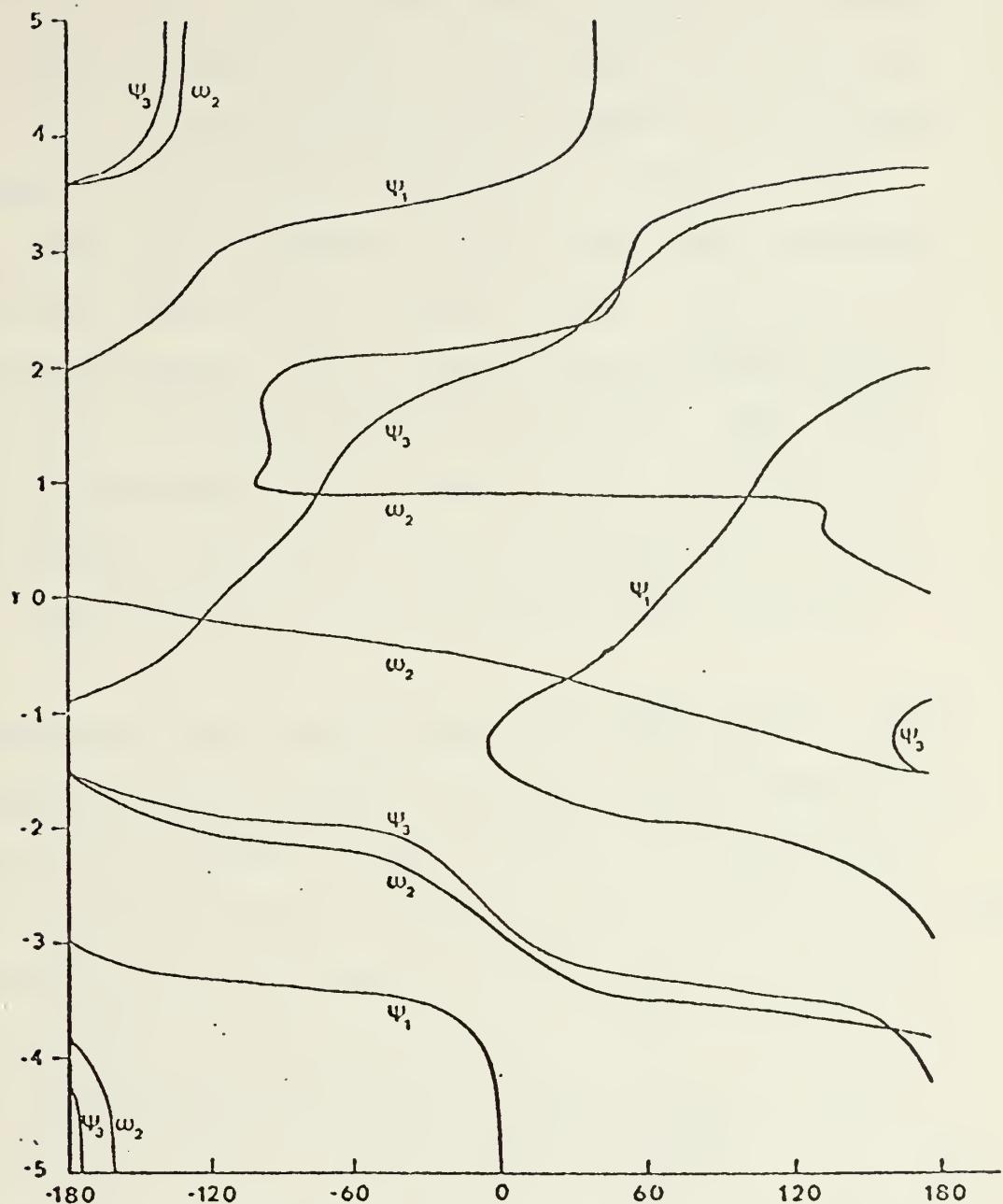
Fig. 14   Phases of ψ_1, ψ_3, and ω_2 for experiment
4 in degrees. Each dependent variable
is expressed in the form $P\cos(kx-\delta)$,
where P is the amplitude and δ is the
phase angle.

in their Figure 4A. The amplitudes for cases 2 and 3 are
not shown but they are much the same as Figure 16. Figure
17 contains the phases of ψ_1, ψ_3, ψ_T, and ω_2 as functions
of y. ψ_T and ω_2 are approximately 165 degrees out-of-phase.
This implies a baroclinic conversion of kinetic energy.
However, the tilt is opposite to the shear which indicates
a barotropic conversion of kinetic energy. The tilt is
westward with height north of the ITCZ and eastward with
height south of the ITCZ which is consistent with rising
motion and unsettled weather that is often observed east
of the surface trough axis in easterly waves north of the
ITCZ. These results are also consistent with those of
WSN.

Experiment 6 was run with the (4.2) wind profile, CISK
heating and surface friction. The beta term and horizontal
friction were excluded. Figure 18 shows the growth rates
for this experiment with a maximum unstable mode at $ky_0 = 1.10$
corresponding to a doubling time of 0.41 days and a wave-
length of 2285 km. The growth rate of 0.790 is similar to
that of experiment 1 and again the large value was due to
the large value of η. The perturbations between wave numbers
0.10 and 1.10 are even larger than in experiment 1 indicating
that there is no clearly defined unstable mode in y. The
amplitudes have a pattern similar to Figure 4. The phases
for this experiment tilted northeast as in the other cases.
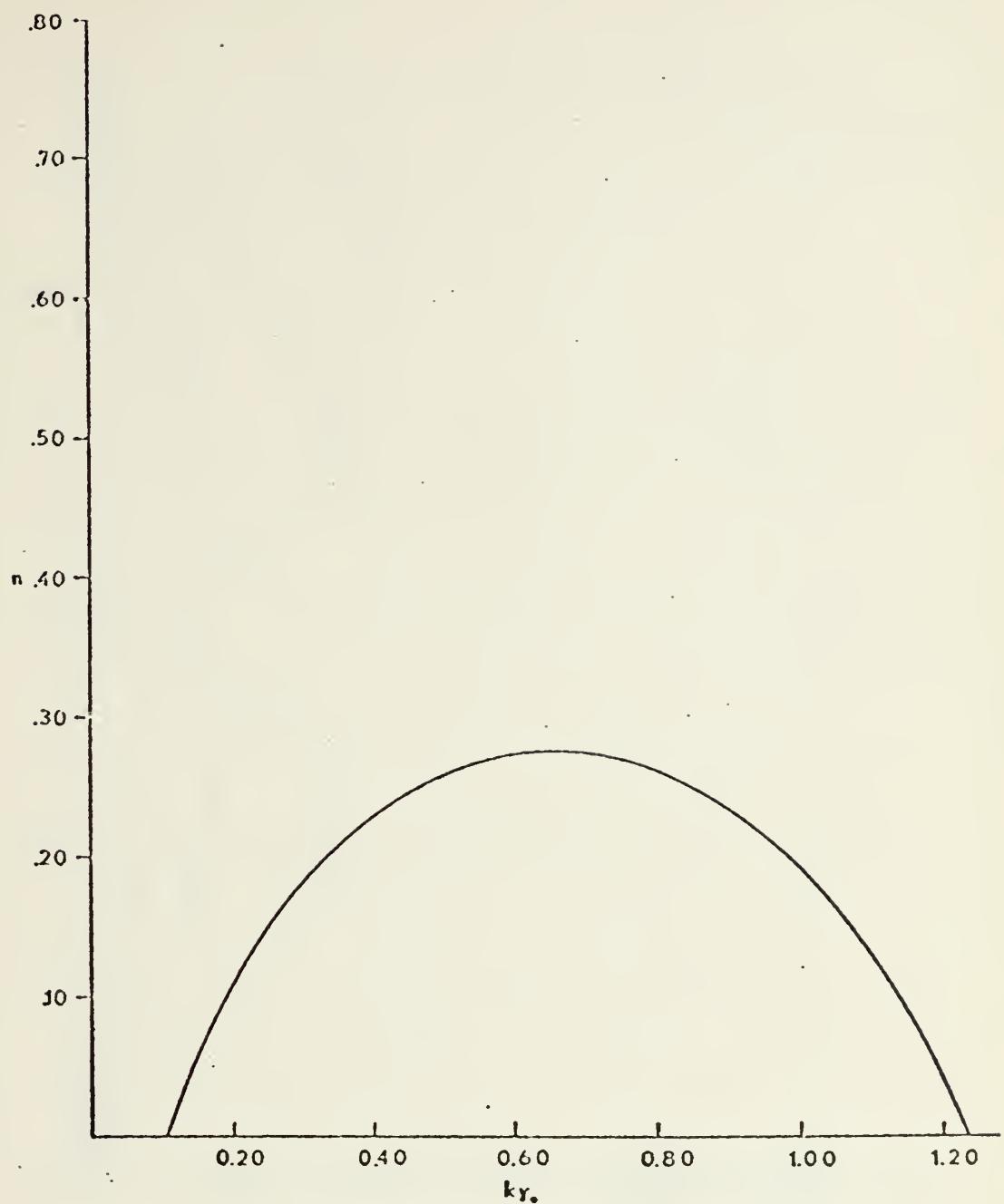
Fig. 15 Growth rates for experiment 5, case 1.
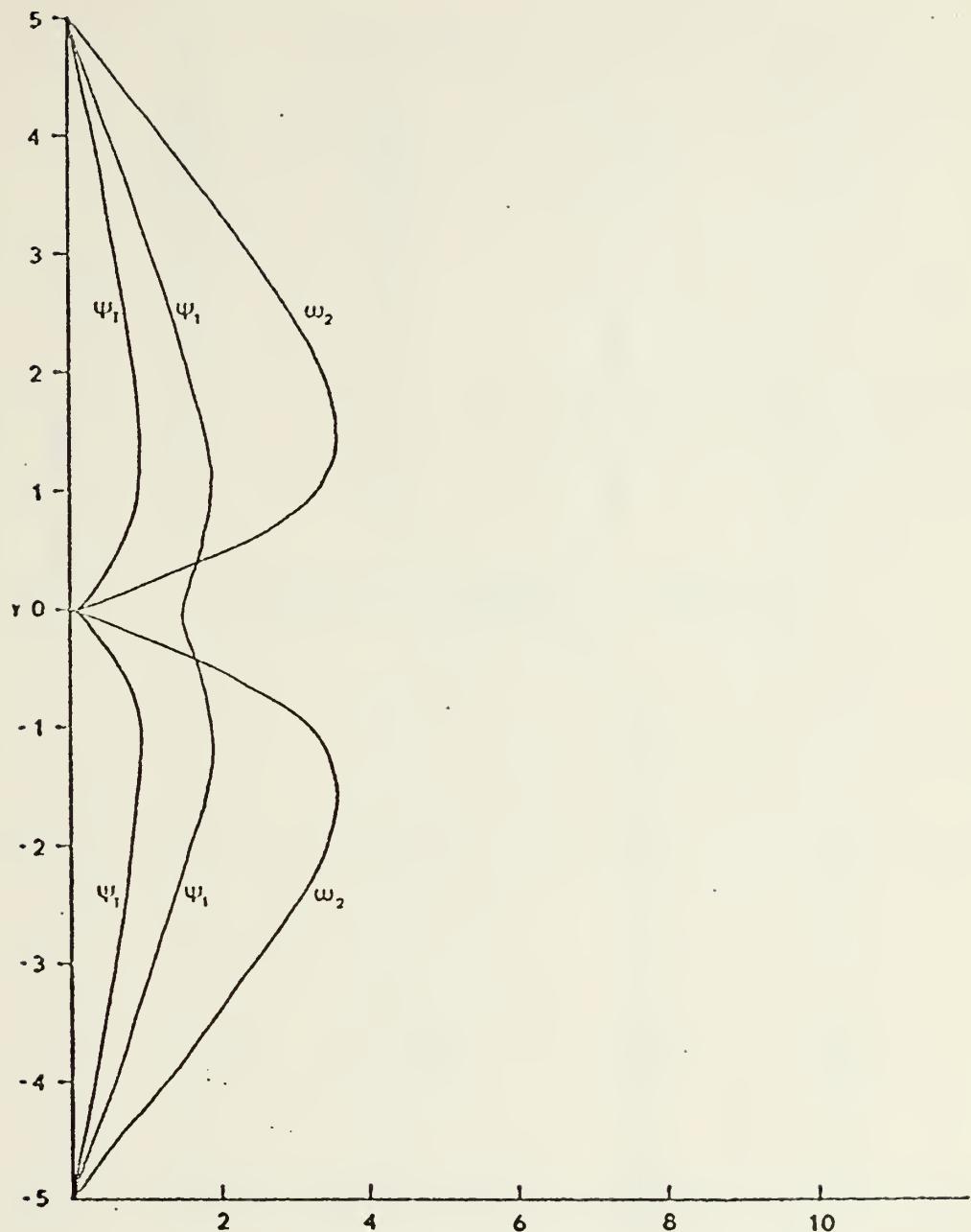
Fig. 16 Amplitudes of ψ_1, ψ_T, and ω_2 for experiment 5, case 1. The quantities ψ_1 and ψ_T have the same scale; ω_2 is on a different scale.
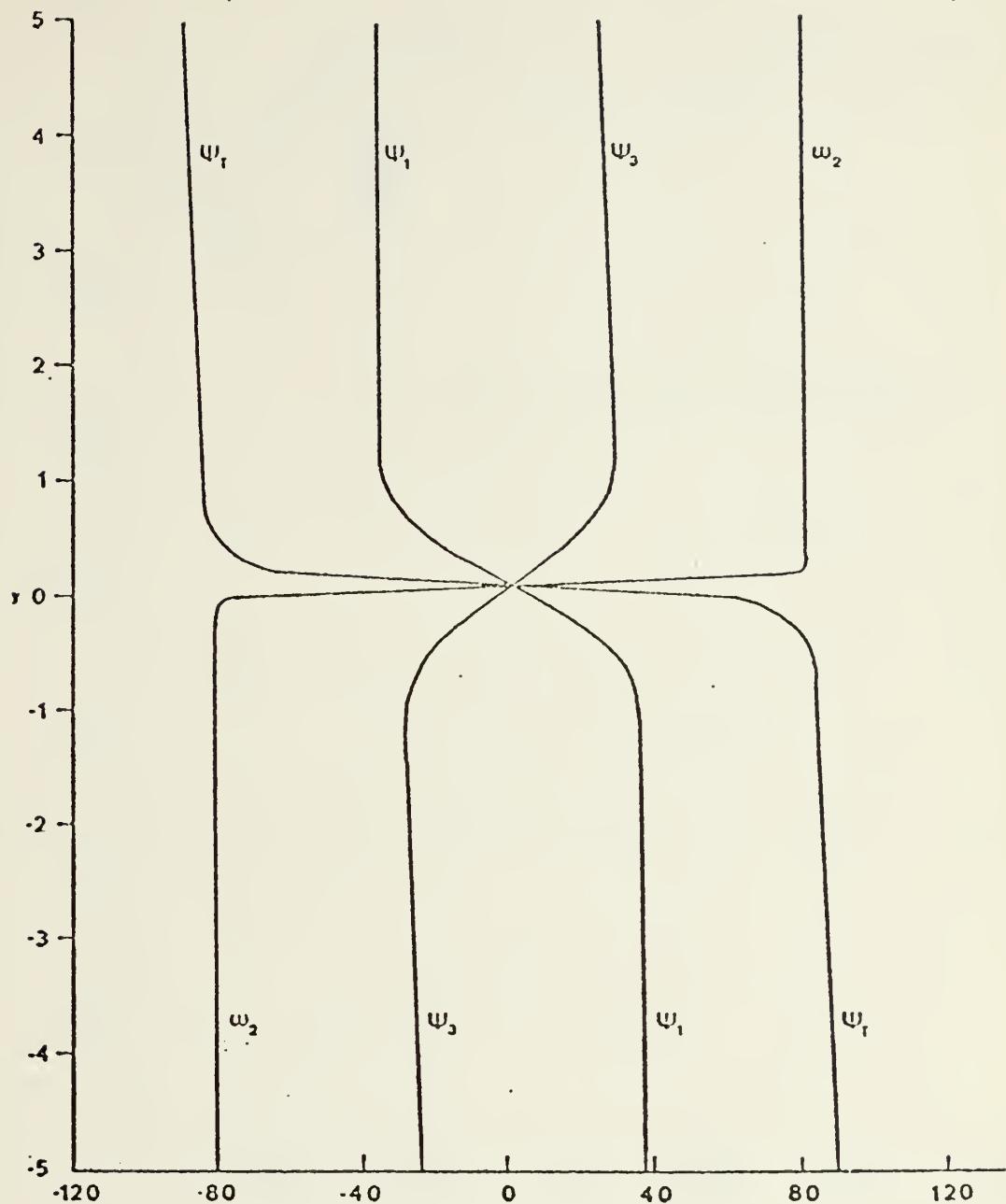
Fig. 17 Phases of ψ_1, ψ_3, ψ_T, and ω_2 for experiment 5, case 1 in degrees. Each dependent variable is expressed in the form $P\cos(kx-\delta)$, where P is the amplitude and δ is the phase angle.

.80

.70

.60

.50

n .40

.30

.20

.10

0.50   1.00   1.50   2.00   2.50   3.00

k γ.
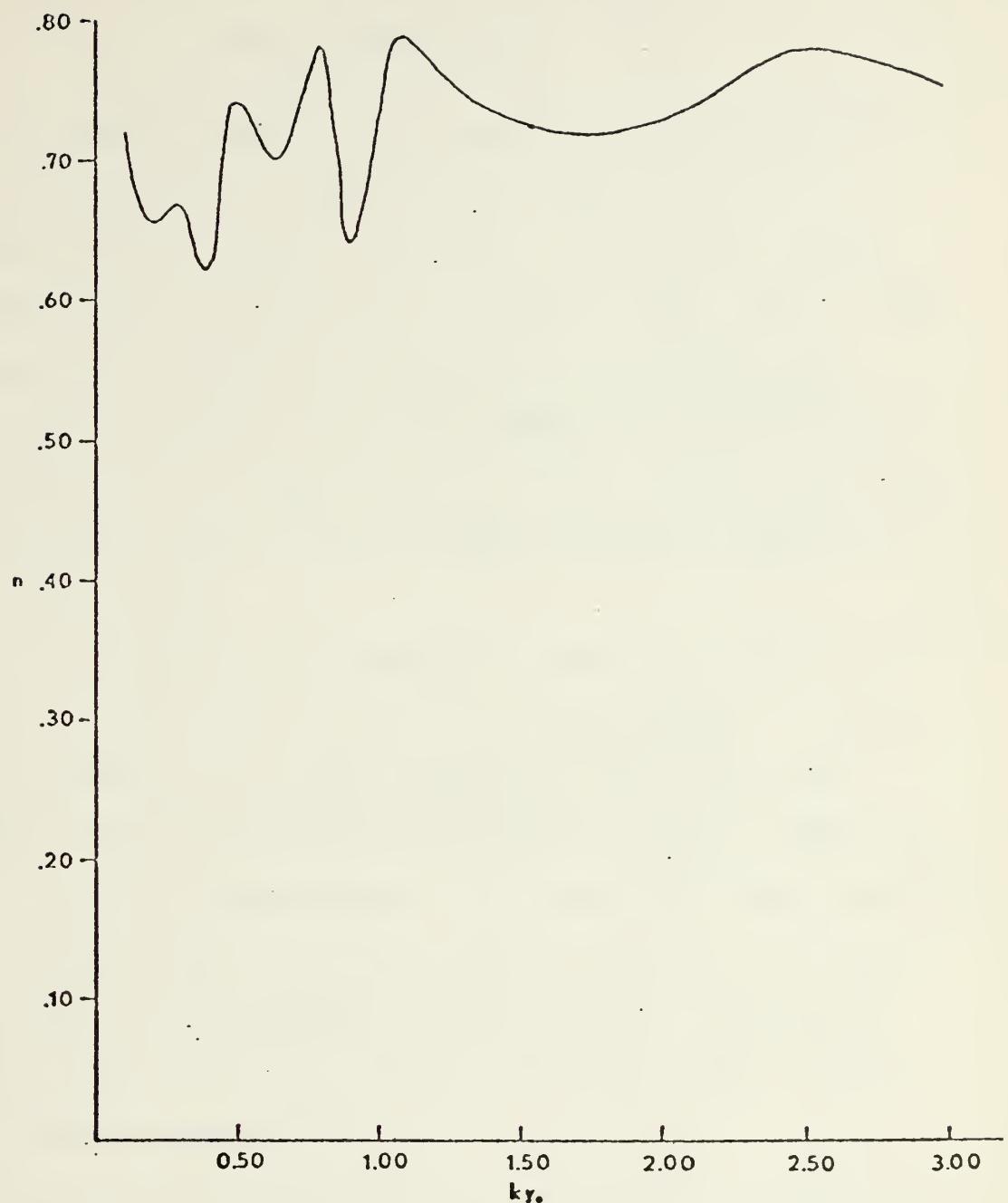
Fig. 18   Growth rates for experiment 6.

VII. CONCLUSIONS

In this thesis, numerically computed barotropically un-
stable disturbances are compared with tropospheric waves
that occur in the tropical easterlies. A two-level quasi-
geostrophic model is used with an attached Ekman layer. The
most unstable solutions are obtained numerically by the
initial value procedure. Two basic shear zone profiles are
used: (1) $\overline{U}_1 = \overline{U}_3 = -U_o$ tanh y/y_o and (2) $\overline{U}_1 = -\overline{U}_3 = U_o$ tanh y/y_o.
Calculations were made in which CISK heating and horizontal
friction were added.

Certain features of the predicted wave structures do
correspond to observed tropical wave disturbances. The tilt
of the disturbance in a sense opposite to the horizontal
wind shear that was observed by Wallace and Chang (1969) is
present in all the experiments. All experiments which contain
heating have the warm structure which was observed by Chang
et al. (1970). The presence of rising motion to the east
of the wave axis which was noted by Yanai and Nitta (1967)
is observed in experiment 5.

The growth rates obtained with heating are unrealistically
large, but it was shown that these could be greatly reduced
by choosing a smaller value of the parameter η. It was also
noted that when heating is present there is no truely
preferred scale of instability. This has been observed by
Chang (1971). It was pointed out in the Introduction that,

while mature tropical wave disturbances may be driven by CISK heating, they may originate from barotropic instability (Bates 1970). If so, then the disturbance should retain certain features (latitude structure, wavelength, etc.) of the barotropically unstable modes. This would provide a selection process which does not occur if CISK heating is present from the start.

The studies of this thesis should be continued but a more complicated model is needed. Proper parameterization of the heating term is necessary. A primitive equation model which includes a better treatment of the boundary layer should be used.

LIST OF REFERENCES

1. Bates, J. R. 1970: Dynamics of disturbances on the inter-tropical convergence zone. Quarterly Journal of the Royal Meteorological Society, Vol. 96, 677-701.

2. Betchov, Robert and William O. Criminale, Jr., 1967: Stability of Parallel Flows, Academic Press, New York.

3. Chang, Chih-Pei, Morris, V. F., and Wallace, John M., 1970: A statistical study of easterly waves in the western Pacific: July-December 1964. Journal of the Atmospheric Sciences, Vol. 27, 195-201.

4. Chang, Chih-Pei, 1971: On the stability of low latitude quasi-geostrophic flow in a conditionally unstable atmosphere. Journal of the Atmospheric Sciences, Vol. 28, 270-274.

5. Chang, Chih-Pei, 1973: On the depth of the equatorial planetary boundary layer. To be puslished in the April Journal of the Atmospheric Sciences.

6. Charney, J. G., 1963: A note on large scale motions in the tropics. Journal of the Atmospheric Sciences, Vol. 20, 607-609.

7. Charney, J. G. and Eliassen, Arnt, 1949: A numerical method for predicting the perturbations of the middle-latitude westerlies. Tellus, Vol. 1, 38-54.

8. Charney, J. G. and Eliassen, Arnt, 1964: On the growth of the hurricane depression. Journal of the Atmospheric Sciences, Vol. 21, 68-75.

9. Garcia, R. V., 1956: Barotropic waves in straight parallel flow with curved velocity profiles. Tellus, Vol. 8, 82-93.

10. Holton, James R., Wallace, John M., and Young, J. A., 1971: Boundary layer dynamics and the ITCZ. Journal of the Atmospheric Sciences, Vol. 28, 55-64.

11. Jacobs, Stanley J. and Aksel Wiin-Nielsen, 1966: On the stability of a barotropic basic flow in a stratified atmosphere. Journal of the Atmospheric Sciences, Vol. 23, 682-687.

12. Kuo, Hsiano-Lan, 1949: Dynamic instability of two-dimensional non-divergent flow in a barotropic atmosphere. _Journal of Meteorology_, Vol. 6, 105-122.

13. Kuo, Hsiano-Lan, 1965: On formation and intensification of tropical cyclones through latent heat release by cumulus convection. _Journal of the Atmospheric Sciences_, Vol. 22, 40-63.

14. Lipps, F. B., 1970: Barotropic stability and tropical disturbances. _Monthly Weather Review_, Vol. 98, 122-131.

15. Matsuno, Taroh, 1966: Quasi-geostrophic motions in the equatorial area. _Journal of the Meteorological Society of Japan_, Vol. 44, 25-43.

16. Nitta, Tsuyoshi, 1970: A study of the generation and conversion of eddy available potential energy in the tropics. _Journal of the Meteorological Society of Japan_, Vol. 48, 127-130.

17. Nitta, Tsuyoshi and Yanai, Michio, 1969: A note on the barotropic instability of the tropical easterly current. _Journal of the Meteorological Society of Japan_, Vol. 47, 127-130.

18. Ogura, Y., 1964: Frictionally controlled, thermally driven circulations in a circular vortex with application to tropical cyclones. _Journal of the Atmospheric Sciences_, Vol. 21, 610-621.

19. Ooyama, K., 1964: A dynamical model for the study of tropical cyclone development. _Geofisica Internacional_, Vol. 4, 187-198.

20. Palmer, Clarence Edgar, 1951: Tropical meteorology. _Compendium of Meteorology_, American Meteorological Society, Boston.

21. Richtmyer, R. D., 1957: _Difference Methods for Initial Value Problems_, Interscience Publishers, Inc., New York.

22. Riehl, Herbert, 1954: _Tropical Meteorology_, McGraw-Hill Book Company, Inc., New York.

23. Starr, Victor P. and Wallace, John M., 1964: Mechanics of eddy processes in the tropical troposphere. _Pure and Applied Geophysics_, Vol. 58, 138-144.

24. Wallace, John M. and Chang, Chih-Pei, 1969: Spectrum analysis of large-scale wave disturbances in the tropical lower troposphere. Journal of the Atmospheric Sciences, Vol. 26, 1010-1025.

25. Williams, R. T., Schminke, T. K., and Newman, R. L., 1971: Effect of surface friction on the structure of barotropically unstable tropical disturbances. Monthly Weather Review, Vol. 99, 778-785.

26. Yamasaki, Masanori, 1969: Large-scale disturbances in the conditionally unstable atmosphere on low latitudes. Papers in Meteorology and Geophysics. Vol. 20, 289-336.

27. Yamasaki, Masanori, and Wada, M., 1972: Vertical structure of the barotropic unstable wave in a tropical easterly current. Journal of the Meteorological Society of Japan, Vol. 50, 271-283.

28. Yanai, Michio and Nitta, Tsuyoshi, 1967: Computation of vertical motion and vorticity budget in a Caribbean easterly wave. Journal of the Meteorological Society of Japan, Vol. 45, 444-466.

29. Yanai, Michio and Nitta, Tsuyoshi, 1968a: Finite difference approximations for the barotropic instability problem. Journal of the Meteorological Society of Japan, Vol. 46, 389-403.

INITIAL DISTRIBUTION LIST

No. Copies

1. Defense Documentation Center   2
   Cameron Station
   Alexandria, Virginia   22314

2. Library, Code 0212   2
   Naval Postgraduate School
   Monterey, California   93940

3. Professor R. T. Williams, Code 51Wu   10
   Department of Meteorology
   Naval Postgraduate School
   Monterey, California   93940

4. Lieutenant Terry G. Robertson, USN   5
   1215 N. E. 86th Avenue
   Vancouver, Washington   98664

5. Navy Weather Service Command   1
   Washington Navy Yard
   Washington, D. C. 20390

6. Officer in Charge   1
   Environmental Prediction Research Facility
   Naval Postgraduate School
   Monterey, California   93940

7. Commanding Officer   1
   U. S. Fleet Weather Central
   COMNAVMARIANAS, Box 12
   FPO San Francisco, California   96630

8. Commanding Officer   1
   Fleet Weather Facility
   P. O. Box 85
   Naval Air Station
   Jacksonville, Florida   32212

9. Commanding Officer   1
   U. S. Fleet Weather Facility
   Box 72
   FPO New York, New York   09510

10. Commanding Officer   1
    Fleet Numerical Weather Central
    Naval Postgraduate School
    Monterey, California   93940

11. Commanding Officer   1
    U. S. Fleet Weather Central
    Box 110
    FPO San Francisco, California   96610

12. Commanding Officer   1
    U. S. Fleet Weather Central
    Box 31
    FPO New York, New York   09540

13. Commanding Officer   1
    U. S. Fleet Weather Facility
    Box 30
    FPO San Francisco, California -96652

14. AFCRL - Research Library   1
    L. G. Hanscom Field
    Attn: Nancy Davis/Stop 29
    Bedford, Massachusetts   01730

15. Director, Naval Research Laboratory   1
    Attn: Tech. Services Info. Officer
    Washington, D. C.   20390

16. Department of Meteorology   3
    Code 51
    Naval Postgraduate School
    Monterey, California   93940

17. Department of Oceanography   1
    Code 58
    Naval Postgraduate School
    Monterey, California   93940

18. American Meteorological Society   1
    45 Beacon Street
    Boston, Massachusetts   02128

19. Office of Naval Research   1
    Department of the Navy
    Washington, D. C.   20360

20. Commander, Air Weather Service   2
    Military Airlift Command
    U. S. Air Force
    Scott Air Force Base, Illinois   62226

21. Atmospheric Sciences Library   1
    National Oceanic and Atmospheric Administration
    Silver Spring, Maryland   20910

22. Professor Victor Starr   1
    Department of Meteorology
    M.I.T.
    Cambridge, Massachusetts   03139

23. Dr. J. Pedlosky   1
    Department of Geophysical Sciences
    University of Chicago
    Chicago, Illinois   60637

24. Dr. Joanne Simpson   1
    Experimental Meteorology Branch
    National Oceanic and Atmospheric Administration
    Coral Gables, Florida   33124

25. Dr. V. Jurcec   1
    Boskoviceva 31/111
    41000 Zagreb
    Yugoslavia

26. Dr. G. C. Asnani   1
    Observatory
    Poona 5, India

27. National Center for Atmospheric Research   1
    Box 1470
    Boulder, Colorado   80302

28. Dr. T. N. Krishnamurti   1
    Department of Meteorology
    Florida State University
    Tallahassee, Florida   32306

29. Dr. Fred Shuman   1
    Director
    National Meteorological Center
    National Oceanic and Atmospheric Administration
    Suitland, Maryland   20390

30. Dr. J. Smagorinsky   1
    Director
    Geophysical Fluid Dynamics Laboratory
    Princeton University
    Princeton, New Jersey   08540

31. Professor N. A. Phillips   1
    Department of Meteorology
    M.I.T.
    Cambridge, Massachusetts   02139

32. Professor J. G. Charney   1
    54-1424
    M.I.T.
    Cambridge, Massachusetts 02139

33. Dr. F. Sanders   1
    Department of Meteorology
    M.I.T.
    Cambridge, Massachusetts 02139

34. Professor K. Ooyama   1
    Department of Meteorology
    New York University
    University Heights
    New York, New York 10453

35. Dr. C. E. Palmer   1
    Institute of Geophysics
    UCLA
    Los Angeles, California 90024

36. Dr. M. G. Wurtele   1
    Department of Meteorology
    UCLA
    Los Angeles, California 90024

37. Dr. A. Arakawa   1
    Department of Meteorology
    UCLA
    Los Angeles, California 90024

38. Captain Thomas Kent Schminke   1
    2107 Randal Drive
    Bellevue, Nebraska 68005

39. Professor H. Riehl   1
    Instutut fuer Meteorologie
    Freie Universitaet Berlin
    Berlin, West Germany

40. Commander R. L. Newman   1
    Fleet Weather Facility
    Box 72
    FPO New York, New York 09501

41. Dr. G. Haltiner   1
    Chairman, Department of Meteorology
    Naval Postgraduate School
    Monterey, California 93940

42. Dr. R. Haney   1
    Department of Meteorology
    Naval Postgraduate School
    Monterey, California 93940

43. Dr. R. Elsberry   1
    Department of Meteorology
    Naval Postgraduate School
    Monterey, California 93940

44. Dr. C. P. Chang   1
    Department of Meteorology
    Naval Postgraduate School
    Monterey, California 93940

45. Dr. R. Renard   1
    Department of Meteorology
    Naval Postgraduate School
    Monterey, California 93940

46. Dr. J. Galt   1
    Department of Oceanography
    Naval Postgraduate School
    Monterey, California 93940

47. Dr. K. Davidson   1
    Department of Meteorology
    Naval Postgraduate School
    Monterey, California 93940

48. Dr. R. Alberty   1
    National Severe Storms Laboratory
    1313 Halley Circle
    Norman, Oklahoma 73069

49. Professor Peter J. Gierasch   1
    Space Sciences Building
    Cornell University
    Ithaca, New York 14850

50. Dr. Peter H. Stone   1
    Institute for Space Studies
    2880 Broadway
    New York, New York 10025

51. Dr. S. Piacsek   1
    Code 7750
    Naval Research Lab
    Washington, D. C. 20390

52. Dr. E. N. Lorenz   1
    Department of Meteorology
    M.I.T.
    Cambridge, Massachusetts   02139

53. Dr. D. Houghton   1
    Department of Meteorology
    University of Wisconsin
    Madison, Wisconsin   53706

54. Dr. S. K. Kao   1
    Department of Meteorology
    University of Utah
    Salt Lake City, Utah   84112

55. Dr. A. P. Ingersoll   1
    Division of Geological and Planetary Sciences
    California Institute of Technology
    Pasadena, California   91109

56. Mrs. O. Haney   1
    Environmental Prediction Research Facility
    Naval Postgraduate School
    Monterey, California   93940

57. Dr. J. Wallace   1
    Department of Atmospheric Sciences
    University of Washington
    Seattle, Washington   98105

58. Dr. J. Holton   1
    Department of Atmospheric Sciences
    University of Washington
    Seattle, Washington   98105   .

59. Dr. J. Young   1
    Department of Meteorology
    University of Wisconsin
    Madison, Wisconsin   53706

60. Dr. T. Ogura   1
    Laboratory for Atmospheric Research
    University of Illinois
    Urbana, Illinois   61801

61. Dr. Y. Sasaki   1
    Department of Meteorology
    University of Oklahoma
    Norman, Oklahoma   73069

62. Dr. J. Mahlman   1
    Geophysical Fluid Dynamics Laboratory
    Princeton University
    Princeton, New Jersey   08540

63. Dr. R. Alexander   1
    The Rand Corporation
    1700 Main Street
    Santa Monica, California   90406

64. Dr. W. L. Gates   1
    The Rand Corporation
    1700 Main Street
    Santa Monica, California   90406

65. Dr. S. Rosenthal   1
    National Hurricane Research Laboratory
    P. O. Box 8265
    University of Miami Branch
    Coral Gables, Florida   33124

66. Mr. Tom Baxter   1
    Environmental Prediction Research Facility
    Naval Postgraduate School
    Monterey, California   93940

67. Dr. F. Lipps   1
    Geophysical Fluid Dynamics Laboratory
    Princeton University
    Princeton, New Jersey   08540

DOCUMENT CONTROL DATA - R & D

(Security classification of title, body of abstract and indexing annotation must be entered when the overall report is classified)

1. ORIGINATING ACTIVITY (Corporate author)	2a. REPORT SECURITY CLASSIFICATION
Naval Postgraduate School Monterey, California 93940	Unclassified
	2b. GROUP

3. REPORT TITLE

Stability of a Tropical Model Including Shear, Surface Friction
and CISK Heating

4. DESCRIPTIVE NOTES *(Type of report and inclusive dates)*
Master's Thesis; March 1973

5. AUTHOR(S) *(First name, middle initial, last name)*

Terry G. Robertson

6. REPORT DATE	7a. TOTAL NO. OF PAGES	7b. NO. OF REFS
March 1973	62	29

8a. CONTRACT OR GRANT NO.	9a. ORIGINATOR'S REPORT NUMBER(S)
b. PROJECT NO.	
c.	9b. OTHER REPORT NO(S) *(Any other numbers that may be assigned this report)*
d.	

10. DISTRIBUTION STATEMENT

Approved for public release; distribution unlimited.

11. SUPPLEMENTARY NOTES	12. SPONSORING MILITARY ACTIVITY
	Naval Postgraduate School Monterey, California 93940

13. ABSTRACT

The structure of barotropically unstable disturbances in the
tropics is studied with a two-level quasi-geostrophic model. An
Ekman layer is attached to the lower boundary. The equations are
linearized and the most unstable mode is found numerically by use
of the initial value technique. CISK heating, horizontal friction
and shear are introduced to give more realistic solutions.
Computations are made for two shear zone wind profiles. The first
is represented by $\overline{U}_1 = \overline{U}_3 = -U_o \tanh y/y_o$ and the second is a mirror
reflection of the first and is given by $\overline{U}_3 = -\overline{U}_1$. The model is run
for 142 days after which growth rates are determined as a function
of the non-dimensional wave number ky_o. The associated phase
angles and amplitudes for the wave numbers with maximum growth
rates are given. The solutions with heating do not have a strongly
preferred mode of maximum growth.

DD FORM 1473 (PAGE 1)
1 NOV 65

S/N 0101-807-6811

Security Classification

A-31408

14 KEY WORDS	LINK A		LINK B		LINK C	
	ROLE	WT	ROLE	WT	ROLE	WT
Barotropic instability						
Two-level model						
CISK heating						
Horizontal friction						
Tropical disturbances						
Vertical shear						

DD FORM 1473 (BACK)